The University of Sydney

Department of Civil Engineering
Sydney NSW 2006
AUSTRALIA

http://www.civil.usyd.edu.au/

Centre for Advanced Structural Engineering

Design Model for Bolted Moment End Plate Connections Joining Rectangular Hollow Sections Using Eight Bolts

Research Report No R827

Andrew Wheeler BE PhD
Murray Clarke BSc BE PhD
Gregory J Hancock BSc BE PhD

March 2003

The University of Sydney

Department of Civil Engineering
Centre for Advanced Structural Engineering
http://www.civil.usyd.edu.au/

Design Model for Bolted Moment End Plate Connections Joining Rectangular Hollow Sections Using Eight Bolts

Research Report No 827

Andrew Wheeler[1], BE, PhD
Murray Clarke[2], BSc, BE, PhD
Gregory J Hancock[3], BSc, BE, PhD

March 2003

Abstract:
In this report a model for the determination of the serviceability and ultimate moment capacities of bolted moment end plate connections utilising rectangular hollow sections joined with eight bolts is presented. The connection configuration is such that two bolts are located above each of the flanges and beside each of the webs. The model considers the combined effects of prying action due to flexible end plates, the formation of yield lines in the end plates, and failures due to punching shear and beam section failure. The model is calibrated and validated using experimental data from a test program.

The design model constitutes a relatively simple method for predicting the serviceability and ultimate moment capacities for the particular type of bolted moment end plate connection described herein.

Keywords:
Tubular, connections, moment end plate, structural design, yield line, prying

---

1 Research Associate, Centre for Construction Technology and Research, The University of Western Sydney, Kingswood, N.S.W. 2747, Australia.

2 Senior Structural Engineer, Mannesmann Dematic Colby Pty Ltd, 24 Narabang Way Belrose, N.S.W. 2085 Australia.

3 BHP Steel Professor of Steel Structures, Department of Civil Engineering, The University of Sydney, N.S.W. 2006, Australia.

Copyright Notice

Department of Civil Engineering, Research Report R827
Design Model for Bolted Moment End Plate Connections Joining Rectangular Hollow Sections using Eight Bolts

Published by:
Department of Civil Engineering
The University of Sydney
Sydney NSW 2006
AUSTRALIA

March 2003

http://www.civil.usyd.edu.au

TABLE OF CONTENTS

Introduction

The increase in the use of rectangular hollow sections in mainstream structures, coupled with the economics of prefabrication, has highlighted the need for simple design methods that produce economical connections for tubular members. In an effort to address this need, the American Institute of Steel Construction has published the document *Hollow Structural Sections Connection Manual* (AISC, 1997), and the Australian Institute of Steel Construction has published the document *Design of Structural Steel Hollow Section Connections* (Syam & Chapman, 1996). Both of these publications present design models for commonly used tubular connections, however the eight-bolt moment end plate connection described in this paper is not included in either one since an appropriate design model did not exist at the time of their publication. Some typical applications of the moment end plate connection using rectangular hollow sections are shown in Figure 1. The eight-bolt connection described in this paper and depicted in Figure 1a represents one of two fundamental bolting arrangements studied by Wheeler (1998). The other bolting arrangement utilises four bolts, as shown in Figure 1b. The eight-bolt detail considered in this paper is superior to the four-bolt variant from the point of view of connection strength and stiffness, but is nevertheless more costly. The design model for the four-bolt tubular end plate connection has been described previously by Wheeler et al. (1998).

There has been little previous experimental or theoretical research on the behaviour of eight-bolt tubular connections subjected to *flexural* loading. Kato & Mukai (1985) utilised yield line analysis to predict the strength of eight bolt tubular end plate connections subjected to pure *tensile* loading. The arrangement of the bolts in the eight-bolt tension connections was similar to that adopted in this paper and resulted in the need to utilise two-dimensional yield line analysis. Three possible failure modes were identified by Kato & Mukai (1985), these

being tensile bolt failure, end plate failure due to excessive deformations, and a combination of end plate deformations and fracture of the bolts. Prying effects were considered in the determination of the bolt capacities.

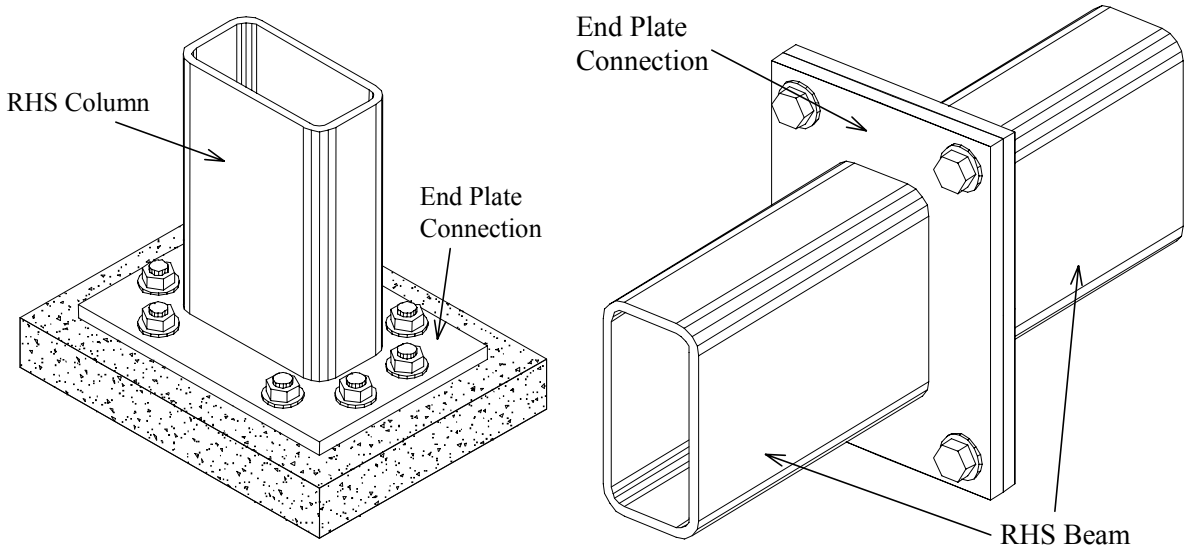

(a) Eight-bolt column base plate connection

(b) Four-bolt beam splice splice connection

Figure 1. Typical applications of bolted moment end plate connections using rectangular hollow sections

Some years later, Kato & Mukai (1991) presented seven modes of failure for eight-bolt connections subjected to combined axial compression and bending. The bolting arrangement was identical to that employed in their earlier work on tensile connections and therefore required two-dimensional yield line analysis. The modes of failure are developed through combined axial compression and flexural loads and comprise the following possibilities: (1) the development of a yield line mechanism in the end plate, without tensile bolt failure; (2) significant yielding in the end plate combined with tensile failure of the bolts; (3) tensile failure of the bolts with one yield line forming in the end plate; and (4) tensile failure of the bolts with no yielding in the end plate.

The effects of prying have been studied extensively and various methods, such as the stub-tee (split tee) analogy (Agerskov, 1976; Kato & McGuire, 1973; Nair *et al.,* 1974; and Kennedy *et al.,* 1981), have been developed to predict the

effects of prying on the connection strengths. These methods have primarily been associated with moment end plate connections in I-sections. While the behaviour of an end plate connection utilising rectangular hollow sections differs from that for an I-section, the stub-tee analogy can be adapted to model the former connection. In the case of eight-bolt tubular connections, the two-dimensional end plate bending significantly complicates the prying phenomenon. The model developed in this paper therefore incorporates an approximate treatment whereby prying is analysed independently in two orthogonal directions. The resulting model is termed the *cumulative stub tee* model.

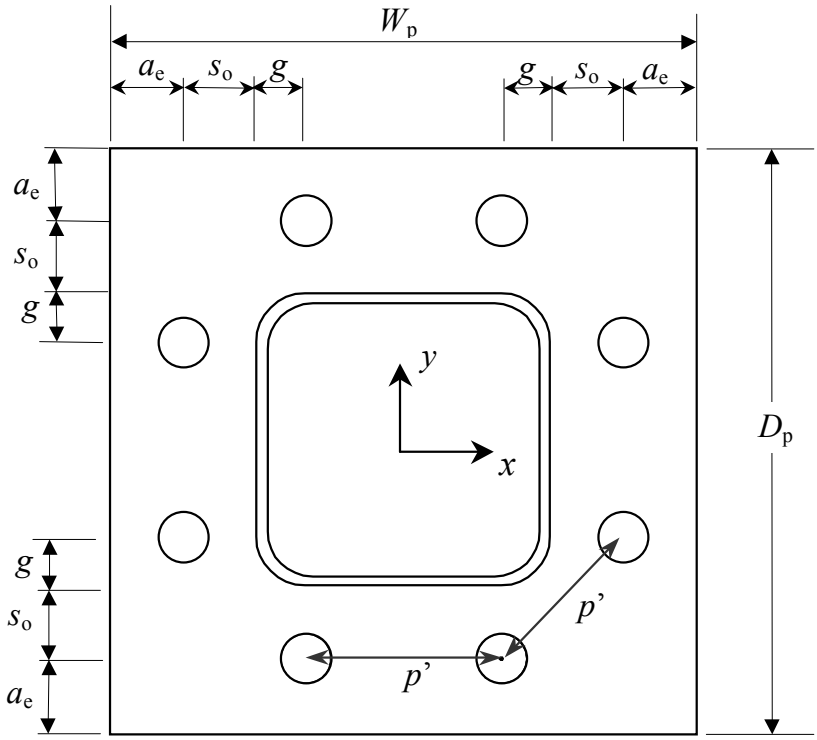

Figure 2. Eight-bolt end plate layout

In this paper, a theoretical model is developed for the analysis of eight-bolt tubular end plate connections subjected to flexural loading. This model is similar to that developed in Wheeler et al. (1998) for a four-bolt tubular end plate connection, where yield line analysis is used to predict the yield moment, and a modified stub-tee analysis to predict the ultimate strength of the

connection. For the eight bolt connection, as defined in Figure 2, additional failure modes involving two dimensional plate yielding or bolt fracture, plastic section failure and punching shear failures were also observed in the experimental programme. These additional modes of failure are considered in the theoretical model developed in this paper. The predictions of the model are compared with the results obtained from an associated experimental program conducted at the University of Sydney (Wheeler *et al*., 1995, 1997, 1998).

Experimental Study

An experimental programme on tubular moment end-plate connections has been conducted at the University of Sydney (Wheeler et al., 1995, 1997). Two basic connection configurations, termed Type A and Type B, were investigated. The Type A connections utilised eight bolts, while the Type B connections employed only four bolts. This report deals solely with the Type A (eight-bolt) connections, having a general configuration as shown in Figure 2. The connections were tested in pure bending, by subjecting a beam containing a beam splice connection (of the type shown in Figure 1b, although containing eight bolts) at mid span to four-point bending.

Table 1. End Plate Connection Details and Test Results

Specimen	Section	Plate Dimensions (mm)					Bolt Length	M_{cu}	Failure
No.	Type†	t_p	W_p	D_p	s_o	g	l_B	(kN.m)	Mode*
1	SHS	16	280	280	35	30	75	116.0	Bolt
2	RHS	16	230	330	35	15	75	124.5	Punching
3	SHS	12	280	280	35	30	75	93.9	Bolt
4	SHS	20	280	280	35	30	90	116.0	Bolt
5	RHS	12	230	330	35	15	75	92.7	Punching
6	RHS	20	230	330	35	15	90	136.7	Bolt
7	SHS	16	260	260	25	35	75	113.2	Bolt
8	SHS	16	300	300	45	25	75	97.6	Punching
9	RHS	16	210	310	25	20	75	133.0	Punching
10	RHS	16	250	350	45	10	75	119.3	Punching

† Section dimensions are given in Table 3.

* Punching = Failure by section tearing away from plate at toe of weld (punching shear)
Bolt = Failure by bolt fracture.

The parameters varied in the experimental programme include the plate size (W_p, D_p), the plate thickness (t_p), the section shape (square or rectangular), and

the positions of the bolts with respect to the section flange and web (s_o and g). The dimensions of the end plates and the type of sections (square (SHS) or rectangular (RHS)) used for all Type A specimens are given in Table 1. The distance from the edge of the plate to the centre of the bolts (a_e) was constant for all tests and set at 30 mm according to the edge distance limits specified in the Australian Standard for Steel Structures, AS 4100 (SA, 1990). All holes were clearance holes (diameter 22mm) for M20 bolts. The end plate material was 350 Grade steel to AS 3678 (SA, 1981b) with a nominal yield stress of 350 MPa. The measured static yield stress (f_y) and ultimate tensile strength (f_u) for each end plate obtained through coupon tests are listed in Table 2.

Table 2. Measured End Plate Material Properties

Plate Thickness t_p (mm)	f_y (MPa)	f_u (MPa)
12	354	499
16	349	482
20	351	496

To eliminate the possibility of the connection strength being limited by local buckling within the beam, all sections used were compact. The nominal section sizes are shown in Table 3, as are the measured ultimate moment capacities (M_{us}) for each type of section. The sections were manufactured by cold forming to the requirements of AS 1163 (SA, 1991a), with a nominal yield stress of 350 MPa.

Table 3. Section Details

Section	Depth d (mm)	Width b (mm)	Thickness t_s (mm)	M_{us} (kN.m)
SHS	151.0	150.9	9.0	119
RHS	199.5	101.5	9.1	138

The bolt and nut assemblies were M20 structural grade 8.8 assemblies (Grade 8.8/T), manufactured to AS 1252 (SA, 1981a). The measured yield and ultimate tensile loads of the bolts were 195 kN and 230 kN, respectively.

The connections were prefabricated to AS 4100 (SA, 1990) using a combination fillet/butt weld joining the section to the end plate. This weld was SP category and qualified to AS 1554.1 (SA, 1991b) with a nominal leg length of 8 mm for the fillet.

Upon assembly of the connection, the bolts were tensioned to the specified proof load of 145 kN (60 per cent of ultimate bolt load). An incremental load was then applied to the connection by means of a stroke-controlled servo until failure occurred. As the sections were not susceptible to local buckling, the ultimate load of the specimen was limited to either connection failure or section failure. The former was deemed to have occurred when the tensile bolts fractured, punching shear failure was observed, or the end plate deformations were deemed excessive. Section failure occurs when a plastic hinge forms in the section. The ultimate moment (M_{cu}) and the failure mode for each test are listed in Table 1.

The results from the experimental programme demonstrated that changes in the end plate width (W_p) and thickness (t_p) resulted in significant changes to the connection ultimate load. An increase in plate thickness (t_p) increased the strength of the joint. The effect of the position of the bolts was demonstrated through their proximity to the section flange (parameter s_o in Table 1). As the bolts were moved closer to the flange of the section, the connection stiffness and strength also increased.

General Theoretical Basis of Model

Theoretical models for the bolted tubular moment end-plate connection based on yield line analysis, the stub-tee analogy, plastic section strength and punching shear are presented in the following sections. A generalised connection model for predicting the ultimate capacity of the connection involving the integration of both the yield line and stub-tee analysis is subsequently derived.

The yield line analysis serves to provide an estimate of the experimental yield moment of the connection* (M_{cy}), which is defined here as the intersection of the initial connection stiffness and the strain hardening stiffness as shown in Figure 3. At the connection yield moment, the end plate is assumed to contain a plastic mechanism characterised by yield lines which form when the end plate cross-section becomes fully plastic at the yield stress f_y. Prying action is not considered in the yield line analysis. As defined here, the connection yield moment may be considered to correspond to the serviceability limit state of the connection.

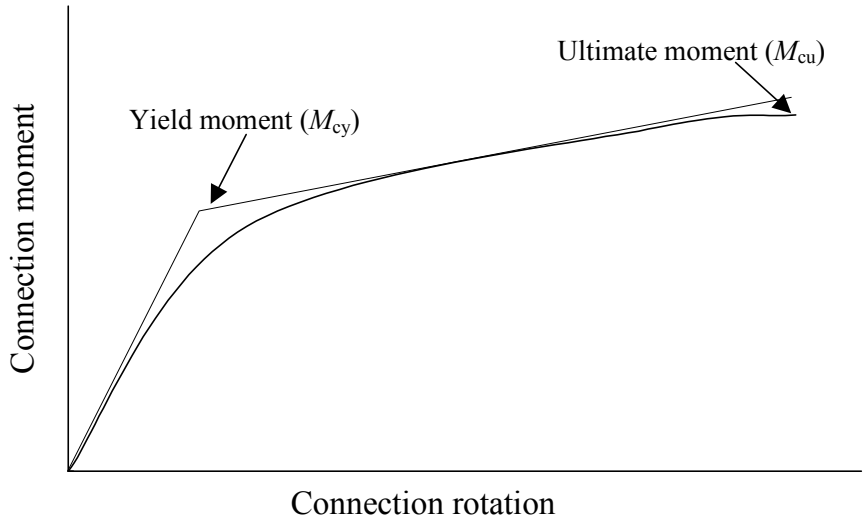

Figure 3. Typical connection moment-rotation curve

* The yield moment (M_{cy}) as defined here should not be confused with the moment to cause first yield of the connection.

The theoretical model based on the stub-tee analogy considers the effects of prying action and aims to predict the experimental ultimate strength of the connection (M_{cu}). The stub-tee analogy is most straightforward to apply when yield lines form in a one-dimensional fashion across the width of the end plate (Agerskov, 1976; Kato & McGuire, 1973). While this is a reasonable assumption for the majority of the four-bolt end plate connections studied by Wheeler et al. (1998), it is not appropriate for the eight-bolt end plate connections described in this report. The end plates in eight-bolt connections invariably experience two-dimensional bending with the formation of inclined yield lines. The incorporation of prying action effects in this context of two-dimensional bending necessitates a component-wise approach in which the stub-tee analogy is applied independently for prying actions in orthogonal directions. For the actions acting in the plane of bending a "Vertical Beam" is utilized, while the actions orthogonal to the plane of bending a "Horizontal Beam" employed. The proposed method is termed the "cumulative stub-tee model".

Since the yield lines invariably undergo significant rotations prior to the connection ultimate strength being reached, much of the material is stressed into the strain-hardening range. For the purpose of predicting the connection *ultimate* moment, it is therefore appropriate to assume the yield lines are fully plastic and stressed to a level denoted f_p which is greater than the yield stress f_y but less than the ultimate tensile strength f_u.

Yield Line Analysis

The various plastic mechanisms considered in the yield line analysis are depicted in Figure 4. As can be gauged from this figure, in many cases the yield line patterns are relatively complicated and make for lengthy expressions for the collapse moment (M_{yl}). For brevity, the derivations of collapse moments are not given in the main part of this report; interested readers may refer to Appendix A for full details. Evaluation of the expressions for the collapse mechanisms for the given plate layouts are presented in Table 4. Of the seven mechanisms shown in Figure 4, Mode 2 is critical for one case. While the calculated collapse moments for Modes 4 and 5 are virtually identical, Mode 4 tends to govern for the square sections and Mode 5 for the rectangular sections. Also included in Table 4 is the calculated yield moment of the section (Mode 8). In the last column of Table 4, M_{yl} is the lower of all the predicted collapse moments (Modes 1 to 8), and M_{cy} is the experimentally determined yield moment as listed in the second column.

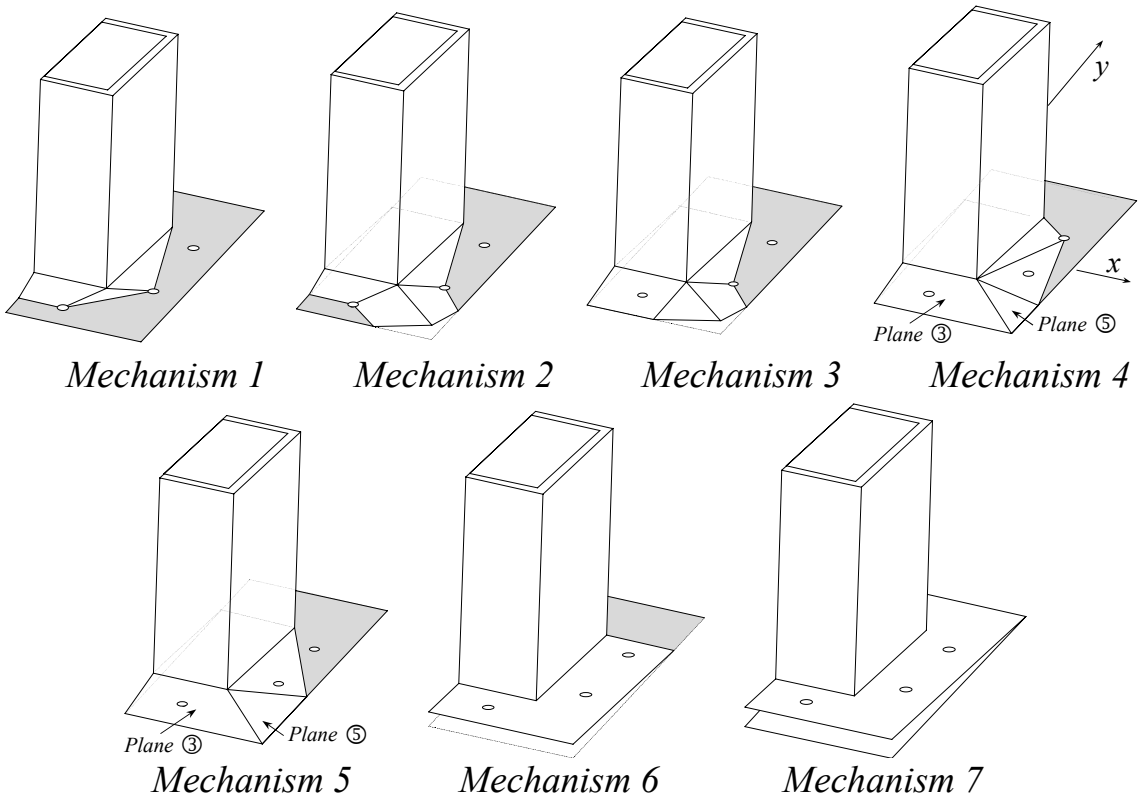

Figure 4. Plastic collapse mechanisms for eight-bolt connection

The results presented in Table 4 allude to the effect of the section shape on the mode of failure of the connection. For the square hollow sections, where the vertical separation of the bolts is comparatively small compared with the rectangular sections (compare Test #1 and Test #2) the dominant failure mode was Mode 4. Test #3, consisting a square section and 12 mm end plate, failed due to Mode 2, which does not involve bolt yielding. The increased vertical separation of the bolts in the RHS connections resulted in all the RHS connections collapsing according to Mode 5.

Table 4. Yield line Analysis Results for Eight-Bolt Connections

Test #	Experimental Yield Moment M_{cy} (kNm)	Calculated Yield Moment M_{yl} (kNm)								M_{yl}/M_{cy}
		Mode 1	Mode 2	Mode 3	Mode 4	Mode 5	Mode 6	Mode 7	Mode 8*	
1 (SHS)	93.9	413.4	122.0	118.4	102.3	105.7	138.3	153.9	104.4	0.92
2 (RHS)	98.6	202.8	197.3	190.6	132.0	132.0	176.5	196.3	117.1	0.84
3 (SHS)	66.6	232.6	68.6	78.6	81.4	79.0	135.5	153.9	104.4	0.97
4 (SHS)	98.0	646.0	190.6	169.7	129.2	129.2	141.8	153.9	104.4	0.94
5 (RHS)	68.7	114.0	111.0	123.1	106.1	106.1	174.3	196.3	117.1	0.65
6 (RHS)	102.0	316.8	308.3	277.3	165.3	165.3	179.4	196.3	117.1	0.87
7 (SHS)	94.2	N/A	144.6	140.2	115.8	116.4	133.9	149.9	104.4	0.90
8 (SHS)	73.3	150.9	109.0	105.1	92.6	92.7	142.7	157.6	104.4	0.79
9 (RHS)	109.0	466.9	239.8	233.8	149.9	149.9	172.2	191.6	117.1	0.93
10 (RHS)	94.0	152.6	171.7	164.1	119.3	119.0	180.9	200.6	117.1	0.80
									Mean	0.86
									S.D.	0.10

* Mode 8 is the yield moment for the beam section determined using the measured moment-rotation relationship.

The comparisons of the predicted yield moments (M_{yl}) and the experimental yield moments (M_{cy}) shown in Table 4 demonstrate that the simplified yield line analysis described in this paper generally overestimates the yield moment of the connection as demonstrated by a mean of 0.86. These errors are attributed to the

simplifications inherent in the yield line models, and the approximate nature of the identification of the experimental yield moments (see Figure 3).

While the yield line analysis developed in this section is not ideally suited to the prediction of yield moments for the eight-bolt connections, it is critical in determining the length of yield lines to be used in the "cumulative modified stub-tee method" described hereafter. It may be possible to obtain more accurate predictions of the yield moments using more complex yield patterns (i.e. curved yield lines and rounded section corners), such yield line models are not investigated in this report.

Cumulative Modified Stub-Tee Method

General

Various stub-tee analogies which consider the effects of prying forces have been developed by previous researchers (Nair et al., 1974; Kennedy et al., 1981) to enable the strength of an end plate connection to be determined. These methods are currently used for moment end plate connections comprising I-sections, and involve a simple rigid plastic analysis of an analogous beam that represents the one-dimensional behaviour of the end plate with yield lines parallel to the axis of bending only. As described in Wheeler et al. (1998), a modification of this approach was employed for the analysis of the four-bolt tubular connections, for which the end plate bending behaviour is also predominantly one-dimensional.

In the eight-bolt tubular end plate connections, bending in the end plate occurs about two axes, with the yield lines not necessarily being parallel to either axis of bending. The stub-tee analysis presented in this section is termed the "Cumulative Modified Stub-Tee Method" and is based on the analysis of analogous beams in both orthogonal directions. The principle of superposition is then used to obtain the resultant connection behaviour.

A simple representation of the two beams used to model the connection behaviour is shown in Figure 5. The "Vertical Beam" analysis (Figure 5a) models the effect of the bolts below the flange of the section, and has an equivalent beam length equal to the plate depth (D_p) and a depth equal to the plate thickness (t_p). Possible plastic hinges are assumed to form at Points 1, 2 and 3. The second analysis, the "Horizontal Beam" (Figure 5b), models the effect of the bolts lying on either side of the section webs. The "Horizontal Beam" has as equivalent length equal to the width of the plate (W_p) and a depth equal to the plate thickness (t_p). Possible plastic hinges are assumed to form at Points 4 and 5 on both sides of the hollow section. To simplify the problem, the

bolts above the neutral axis (in the compressive zone) are assumed to have a negligible effect on the connection strength.

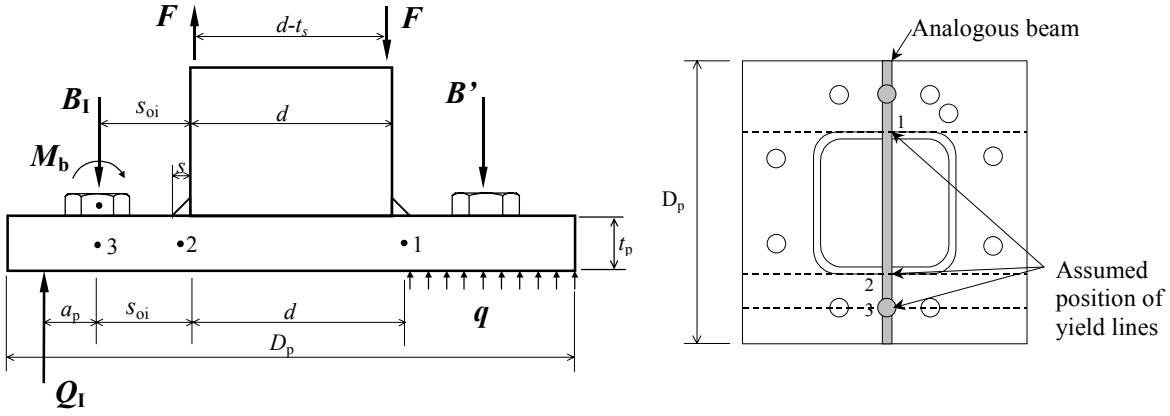

(a) End Plate contributing to "Vertical Beam"

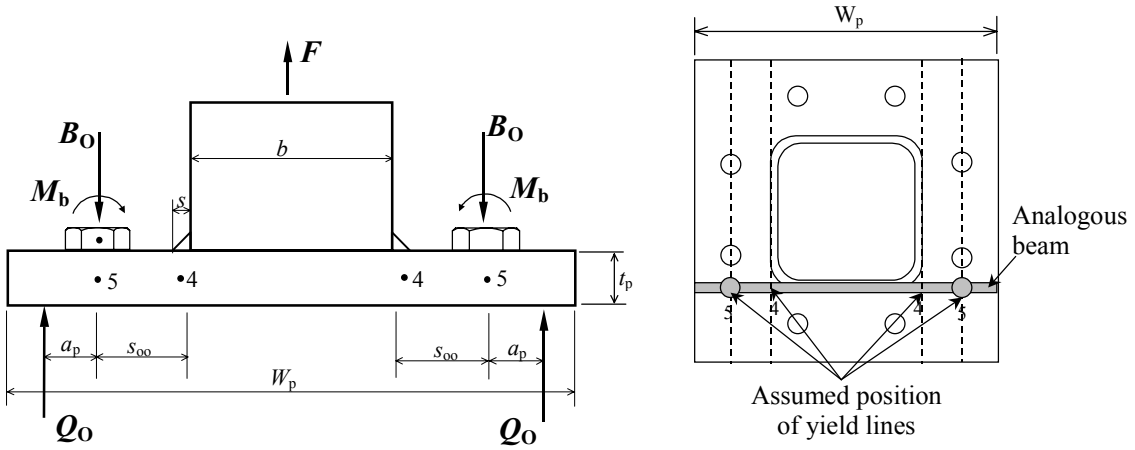

(b) End Plate contributing to "Horizontal Beam"

Figure 5. Analytical model for the eight-bolt connection

The moment acting on the connection (M_c) is assumed to be applied to the end plate through equal and opposite flange forces F acting through the centrelines of the flanges, so that

Error! Objects cannot be created from editing field codes. (1)

The bolts forces are assumed to act through the centre of the bolts and are denoted B_I and B_O for the bolts considered in the "vertical beam" and "horizontal beam", respectively. The moment generated through bending of the individual bolts as a result of the end plate deformation is denoted M_b (defined Equation 12, following).

The prying forces are simplified to point loads (Q_I and Q_O) acting at a distance a_p from the centreline of the bolts. As a reflection of the fact that the end plate thickness and edge distances to the bolts are the same for both analogous beams, the line of action (a_p) to the prying force has been assumed identical for both orthogonal beams. The value for a_p varies significantly depending on the assumptions made. In this report it is assumed that a_p = 25 mm.

The tensile force (F) acting through the tensile flange of the section is expressed in terms of the shear forces either side of the flange, and the shear forces generated in the connection are shown in Figure 6.

$$F = F_R + F_L + 2 \cdot F_O \tag{2}$$

where F_L is the shear force on the left of the tensile flange of the section and F_R the shear force on the right side of the flange. The shear force generated through the "horizontal beam" are denoted F_O.

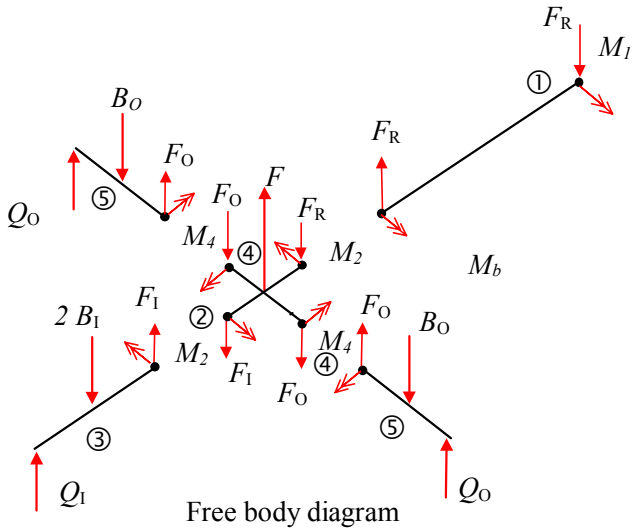

Figure 6. Definition of forces on free-body segment of beam

The shear forces are now expressed in terms of the bolt loads (B_O and B_I), the prying force (Q_O and Q_I) and the internal moments at Points 1 and 2 (M_1, M_2) as

$$F_L = 2 \cdot B_I - Q_I \tag{3}$$

$$F_O = B_O - Q_O \tag{4}$$

$$F_{\mathrm{R}} = \frac{M_1 + M_2}{d} \tag{5}$$

Combining the Equations 1 – 5, the general expression for the connection moment (M_{c}) is obtained as

$$M_{\mathrm{c}} = F \cdot (d - t_{\mathrm{s}}) = \left(2 \cdot B_{\mathrm{I}} - Q_{\mathrm{I}} + 2 \cdot (B_{\mathrm{O}} - Q_{\mathrm{O}}) + \frac{M_1 + M_2}{d} \right) \cdot (d - t_{\mathrm{s}}) \tag{6}$$

The behaviour of the connection may be divided into three categories depending on the thickness of the end plate (t_{p}) and the magnitude of the applied load. These categories are defined as *Thick Plate Behaviour*, *Intermediate Plate Behaviour* and *Thin Plate Behaviour* (Kennedy et. al, 1981), and are identified by the position and number of yield lines. Thick plate behaviour occurs when the connection fails due to bolt fracture prior to yield lines forming at Points 2 or 4. Intermediate plate behaviour occurs when the bolts fracture after the formation of yield lines at Points 1, 2 and 4 (i.e. Plastic Collapse Mechanism 5). Thin plate behaviour corresponds to the formation of yield lines at Points 1, 2, 3, 4 and 5 in the end plate (i.e. Plastic Collapse Mechanism 2), without deformation of the bolts.

The plastic moment (M_{ip}) for each of the "hinges" i shown in Figure 5 is given by

$$M_{i\mathrm{p}} = \frac{1}{4} \cdot t_{\mathrm{p}}^2 \cdot f_{\mathrm{p}} \cdot l_i \tag{7}$$

where t_{p} is the end plate thickness, f_{p} is the (inelastic) stress along the yield line (see Equation 9 following), and l_i is the length of the i th yield line.

The lengths of these yield lines (l_i) depends on the mode of failure. The dominant end plate failure mode for the eight-bolt connection tests was Mode 4 for the SHS and Mode 5 for the RHS, as indicated in Table 4.

The bolts loads are assumed to vary depending on their distance from the yield line forming at the top of the section (Point 1 in Figure 5a). The lower bolts (those beyond the tensile flange of the section) are considered to have obtained their ultimate tensile load. The loads in the next layer of bolts (adjacent to the webs of the section) are assumed to be related linearly to the loads in the extreme tensile bolts according to the distance to the compression flange of the section as given by

$$B_O = h \cdot B_I \quad \text{where} \quad h = \frac{(d-g)}{(d+s_{oi})} \tag{8}$$

Reflecting the influence of strain-hardening at the point of ultimate moment on the connection, and following the approach of Packer et al. (1989), the stress (f_p) used to calculate the plastic moment capacity of the end plate is assumed to be intermediate in value between the yield stress (f_y) and the ultimate tensile strength (f_u) of the plate material,

$$f_p = \frac{f_y + 2 \cdot f_u}{3} \tag{9}$$

In this thesis, f_p is termed the plate design stress.

Thick Plate Behaviour

Thick plate behaviour (Figure 7) is deemed to occur when there is no or very little yielding in the end plate. The upper limit of thick plate behaviour occurs when a mechanism forms through the combination of a yield line across the top of the section, and yielding of the bolts in the tensile region as described by Mechanism 6. The ultimate bolt load ($2 \cdot B_u$) is the tensile resistance produced by the bolts at the bottom of the connection while the remaining tensile bolts in the connection provide a fraction of the ultimate load ($h \cdot B_I$) as defined by Equation 8.

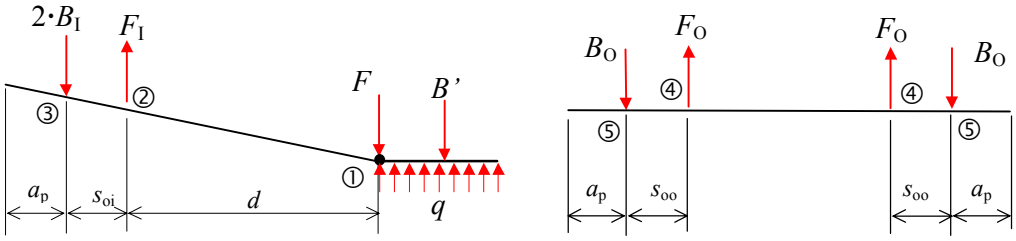

(a) "Vertical Beam" *(b) "Horizontal Beam"*

Figure 7. Thick plate behaviour

For thick plate behaviour, the prying forces (Q_I and Q_O) are zero. Also, since there is little bending in the plate, the resisting moment of the bolts (M_b) is neglected. The moment at Point 2 (M_2) is found by considering moment equilibrium for the left-hand segment of the "Vertical Beam" beam.

$$M_2 = 2 \cdot B_I \cdot s_{oi} \tag{10}$$

From Equation 6 and Equation 10, ignoring the prying forces and M_b, and assuming a plastic hinge forms at Point 1 ($M_1 = M_{1p}$), the ultimate moment capacity of the connection can be expressed as

$$M_{Cthick} = \left(\frac{M_{1p} + 2 \cdot B_I \cdot (d + s_{oi} + h \cdot d)}{d} \right) \cdot (d - t_s) \tag{11}$$

Thick end plate behaviour is considered to hold as long as the moment at Point 2, as calculated from Equation 10, is less than the plastic moment ($M_2 \le M_{2p}$).

Intermediate Plate Behaviour

The mechanism for intermediate plate behaviour, shown in Figure 8, is a combination of bolt yielding and plate yielding.

The mechanism is characterised by plastic hinges forming at Points 1 and 2 along the "vertical beam" and Point 4 in the "horizontal beam". The bolts at Point 3 are deemed to be at yield while the bolt forces at Point 5, are related linearly to the former bolt forces through Equation 8.

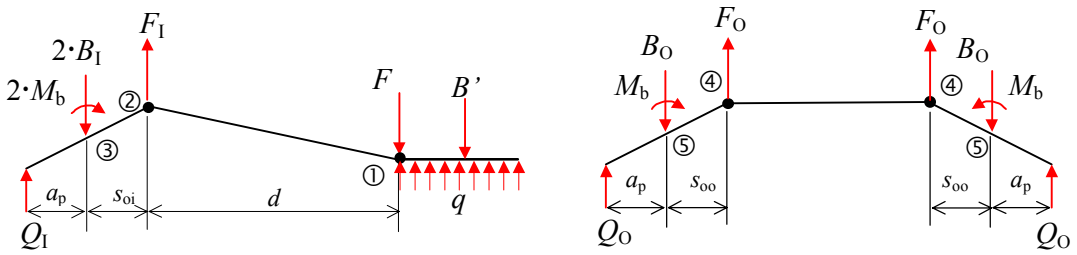

(a) "Vertical Beam" beam *(b) "Horizontal Beam" beam*

Figure 8. Intermediate plate behaviour

The bolts are assumed to have attained their full plastic moment and so the resistance generated by the bending of a single bolt is given by

$$M_b = \frac{\pi \cdot d_b^3 \cdot f_{yb}}{32} \tag{12}$$

where d_b is the bolt diameter and f_{yb} is the bolt yield stress.

The free body diagrams for intermediate plate behaviour are shown in Figure 9. It is assumed that when intermediate plate behaviour commences, the prying forces (Q_I and Q_O) are zero. The prying forces Q_I and Q_O attain their maximum value (Q_{max}) at the point of transition from intermediate to thin plate behaviour. As discussed previously, the yield lines characteristic of intermediate plate behaviour form at Points 1, 2 and 4, thus $M_1 = M_{1p}$, $M_2 = M_{2p}$ and $M_4 = M_{4p}$. In the following description, intermediate plate behaviour is addressed firstly for the limiting case of zero prying force ($Q_I = Q_O = 0$) and then for positive prying force ($Q_I > 0$, $Q_O > 0$).

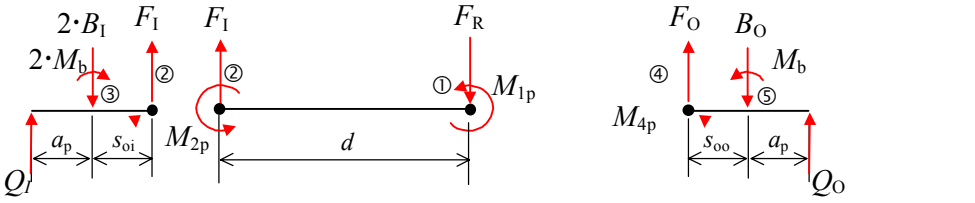

(a) "Vertical Beam" beam *(b) "Horizontal Beam" beam*

Figure 9. Intermediate plate free body diagrams

The two cases of zero and positive prying forces (Q_I and Q_O) are considered separately in the following.

Case 1: Prying force $Q_I = Q_O = 0$

When the prying forces (Q_I and Q_O) are zero, the end plate is in the transition stage from thick to intermediate plate behaviour. At this point, the bolt loads (B_I and B_O) can be determined from Figure 9 by taking moments about Point 2 and Point 4 respectively, giving

$$B_I = \frac{M_{2p} + 2 \cdot M_b}{2 \cdot s_{oi}} \tag{13}$$

$$B_O = \frac{M_{4p} + M_b}{s_{oo}} \tag{14}$$

Substituting Equations 13 and 14 into Equation 6, and setting the prying forces to zero enables the ultimate connection capacity at the point of transition from thick to intermediate behaviour to be expressed as

$$M_{Cint} = \left(\frac{M_{2p} \cdot (d + s_{oi}) + M_{1p} \cdot s_{oi} + 2 \cdot M_b \cdot d}{s_{oi} \cdot d} + 2 \cdot \frac{M_{4p} \cdot d + M_b \cdot d}{s_{oo} \cdot d} \right) \cdot (d - t_s) \tag{15}$$

Case 2: Prying force $Q_I > 0$, $Q_O > 0$

It is assumed that the prying forces Q_I and Q_O become positive concurrently. When the prying forces are greater than zero they can be evaluated using

$$Q_I = \frac{M_3}{a_p} = \frac{F_I \cdot s_{oi} - M_{2p} - 2 \cdot M_b}{a_p} \tag{16}$$

$$Q_O = \frac{M_5}{a_p} = \frac{F_O \cdot s_{oo} - M_{4p} - M_b}{a_p} \tag{17}$$

Substituting Equation 3 into Equation 16 and Equation 4 into Equation 17 enables the prying forces Q_I and Q_O to be determined as

$$Q_I = \frac{2 \cdot B_I \cdot s_{oi} - M_{2p} - 2 \cdot M_b}{a_p + s_{oi}} \tag{18}$$

$$Q_{\mathrm{O}} = \frac{h \cdot B_{\mathrm{I}} \cdot s_{\mathrm{oo}} - M_{3\mathrm{p}} - M_{\mathrm{b}}}{a_{\mathrm{p}} + s_{\mathrm{oo}}} \tag{19}$$

Further substitution of Equations 18 and 19 into Equation 6 results in the expression for the ultimate moment capacity (M_{Cint}) of the connection based on intermediate behaviour with positive prying forces.

$$M_{\mathrm{Cint}} = \left(\frac{2 \cdot B \cdot a_{\mathrm{p}} + M_{2\mathrm{p}} + 2 \cdot M_{\mathrm{b}}}{\left(a_{\mathrm{p}} + s_{\mathrm{oi}}\right)} + 2 \cdot \frac{h \cdot B \cdot a_{\mathrm{p}} + M_{4\mathrm{p}} + M_{\mathrm{b}}}{\left(a_{\mathrm{p}} + s_{\mathrm{oo}}\right)} + \frac{M_{1\mathrm{p}} + M_{2\mathrm{p}}}{d} \right) \cdot \left(d - t_{\mathrm{s}}\right) \tag{20}$$

The above exposition on intermediate plate behaviour is valid from the point when the moment at Point 2, calculated from Equation 10, exceeds the plastic moment ($M_{2\mathrm{p}}$), and while ever the moment at Point 3, calculated from Equation 16, is less than the plastic moment ($M_{3\mathrm{p}}$). These conditions can be expressed in the following equations:

$$2 \cdot B_{\mathrm{I}} \cdot s_{\mathrm{oi}} \geq M_{2\mathrm{p}} \tag{21}$$

$$F_{\mathrm{I}} \cdot s_{\mathrm{oi}} - M_{2\mathrm{p}} - 2 \cdot M_{\mathrm{b}} \leq M_{3} \tag{22}$$

The bolt load B_{I} must also be less than or equal to the ultimate bolt load (B_{u}).

Thin Plate Behaviour

Thin plate behaviour (Figures 10 and 11) occurs when the moments at Points 1, 2 and 3 in the "vertical beam" and the moments at Points 4 and 5 in the "horizontal beam" have reached their plastic limits ($M_{1\mathrm{p}}$, $M_{2\mathrm{p}}$, $M_{3\mathrm{p}}$, $M_{4\mathrm{p}}$ and $M_{5\mathrm{p}}$).

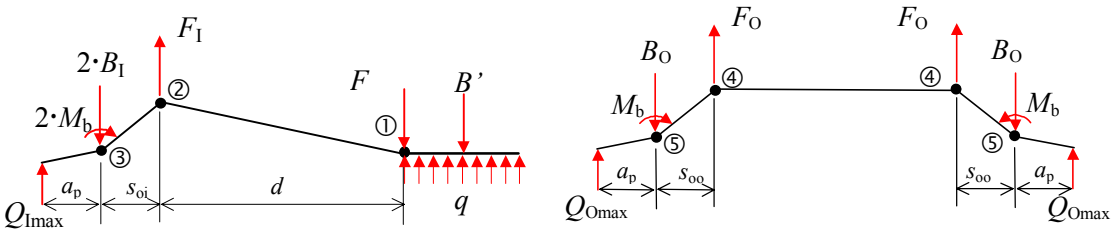

(a) "Vertical Beam" *(b) "Horizontal Beam"*

Figure 10. Thin plate behaviour

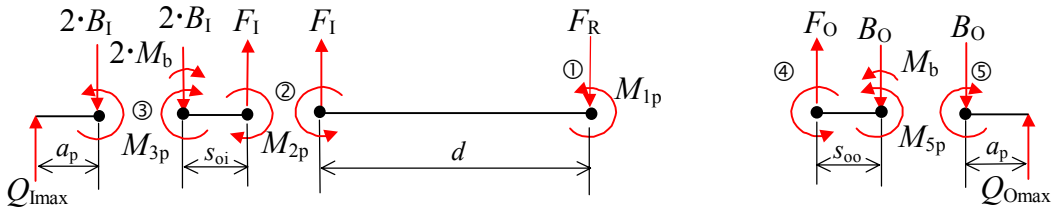

(a) "Vertical Beam" *(b) "Horizontal Beam"*

Figure 11. Thin plate free body diagrams

Compared to intermediate plate behaviour, for thin plates additional yield lines form at Points 3 and 5. Once these yield lines have formed, the prying forces attain their maximum values (Q_{Imax} and Q_{Omax}):

$$Q_{Imax} = \frac{M_{3p}}{a_p} \tag{23}$$

$$Q_{Omax} = \frac{M_{5p}}{a_p} \tag{24}$$

The end plate behaves in an intermediate manner prior to the yield line forming at Point 3. Using Equations 18 and 19 and substituting $Q_I = Q_{Imax}$ and $Q_O = Q_{Omax}$ enables the bolt loads B_I and B_O to be expressed

$$B_I = \frac{Q_{Imax} \cdot (a_p + s_{oi}) + M_{2p} + 2 \cdot M_b}{2 \cdot s_{oi}} \tag{25}$$

$$B_O = \frac{Q_{Omax} \cdot (a_p + s_{oi}) + M_{4p} + M_b}{s_{oo}} \tag{26}$$

The resulting connection moment capacity for thin plate behaviour is found using Equations 25, 26 and 6, and is given by

$$M_{Cthin} = \left(\frac{M_{1p} + M_{2p}}{d} + 2 \cdot \frac{M_{5p} + M_{2p} + M_b}{s_{oo}} + \frac{M_{3p} + M_{2p} + 2 \cdot M_b}{2 \cdot s_{oi}} \right) \cdot (d - t_s) \tag{27}$$

Thin plate behaviour holds while the moment at Point 3 is equal to the plastic limit.

Equivalent Yield Line Lengths

The stub-tee analogy assumes that the yield lines form in a linear fashion, both transversely across the end plate and vertically in the plane of bending. The plastic collapse mechanism analysis, however, indicates that the yield lines rarely occur in this manner for eight-bolt connections. To compensate for this inconsistency, "*equivalent lengths*" (considering bending in the vertical and horizontal directions) are determined for the yield lines such that the total amount of internal work involved in the mechanism remains unchanged.

The equivalent lengths of the yield lines used for the cumulative stub-tee analysis depend on the assumed plastic collapse mechanism. Furthermore, these yield line lengths represent the cumulative length of the x or y components of several yield lines. An example of this is the equivalent yield line at point 2 (Figure 5a) for the plastic collapse Mechanism 5 (see Figure 4). The equivalent length of this yield line is deemed to be the sum of the yield line along the base of the beam section (b), and twice the x component of the diagonal yield line between Planes 3 and 5 (see Figure 4).

Although seven yield line mechanisms were identified and analysed, the test results indicate that the dominant failure modes that represent intermediate plate behaviour are Mechanisms 4 and 5 (Figure 4). To further simplify the problem, in this thesis intermediate plate behaviour is assumed to be based on Mechanism 5, as the results for Mechanism 4 were only marginally

(less than 3%) higher than those given by the former. To describe the thin plate behaviour, it is assumed that the end plate fails according to Mechanism 2, as the results from Mechanism 1 were consistently higher. The resulting equivalent yield line lengths are given in Table 5 and were determined using the yield line

analysis given in Appendix A. The plastic moment capacity (M_{ip}) of the yield line i is then defined by

$$M_{ip} = m_p \cdot l_i \tag{28}$$

where l_i is the equivalent length of yield line i, and m_p is the full plastic moment of the end plate per unit length. The parameter k in the last column of Table 5 should be chosen such that the resulting connection moment capacity M_{cthin} given by Equation 27 is minimised. In practice this minimisation is performed numerically.

Table 5. Equivalent Lengths of Yield Lines for Cumulative Stub-Tee Analysis

Equivalent Yield Line (Figure 5)	Intermediate Plate Equivalent Yield Line Length (Mechanism 5)	Thin Plate Equivalent Yield Line Length (Mechanism 2)
Point 1	b	b
Point 2	$b+2\cdot(s_o+a)$	$b+2\cdot(s_o+a)$
Point 3	N/A	$b-2\cdot g+\frac{2\cdot(s_o+a+g\cdot(1-k))\cdot a}{k\cdot s_o+a}$
Point 4	$d+(s_o+a)$	$d+s_o+a$
Point 5	N/A	$\frac{((d-g)\cdot k+a)\cdot s_o+(a+d-k\cdot g)\cdot a}{k\cdot s_o+a}$

The theoretical capacities for the connections have been determined utilising the cumulative stub tee method as detailed previously. The predicted moment capacities for all three types of end plate behaviour are presented in Table 6, with the governing mode highlighted. The connection dimensions are given in Table 1, and the corresponding end plate material properties are as detailed in Table 2. The bolt yield and ultimate loads are B_{y1} = 197 kN and B_{u1} = 230 kN, respectively. As explained in subsequent sections, although it is not usually

appropriate to compare the stub-tee model results with the test results, the latter values are also given in Table 6 for reference purposes.

Table 6. Connection Ultimate Moments Predicted using Modified Stub-Tee Model

Test	Connection Capacity (kNm)			Experimental Capacity
#	Thick	Intermediate	Thin	M_{cu} (kN)
1	122.8	117.8	168.5	115.1
2	171.9	164.1	217.0	124.6
3	121.1	92.8	98.8	93.9
4	125.0	149.9	258.2	116.0
5	170.8	130.9	127.4	92.7
6	173.4	206.7	332.2	136.7
7	119.2	136.1	234.6	113.2
8	126.4	104.9	136.3	97.6
9	172.8	193.9	308.2	133.1
10	171.6	143.2	172.5	119.3

Plastic Section Capacity

The plastic section capacity of the tubular member may also govern the ultimate moment that the connection can attain. Design specification such as AS 4100 (SA, 1990) generally define the plastic section capacity as the yield stress (f_y) times the plastic section modulus (S). Although appropriate for design, this method of calculating the section plastic capacity does not usually reflect the experimentally measured ultimate moment as the cold working of the section introduces significant strain hardening into the material properties. A more accurate method to predict the experimental plastic section capacity would be to use the allowable stress as defined by Packer *et al.* (1989). The yield stress and ultimate strength are based on a weighted average of the material from the flats and rounds of the section.

$$M_s = S \cdot f_p \tag{29}$$

where S is the plastic section modulus, and f_p is the plate design stress as defined by Equation 9 using the measured yield stress (f_y) and measured ultimate strength (f_u) of the material.

Punching Shear

Punching shear failure (tearing of the end plate) occurs when the concentrated loads transferred from the section to the end plate exceed the shear capacity of the end plate over a localised region. While punching shear was not observed in the four-bolt connections (Wheeler et al., 1998), the additional rigidity of the eight-bolt connections, coupled with the high bending capacity of the section, resulted in the occurrence of punching shear failure in several of these tests.

The model presented in this paper to predict the connection moment at which punching shear failure occurs follows a simplified approach and assumes that shear failure planes are defined by the geometry of the connection. The model also assumes that at the point of punching shear failure, the effect of bending in the end plate is minimal and does not affect the through thickness shear capacity of the end plate. The connection is considered to have failed in punching shear if the load in the tensile flange and adjacent regions of the section exceeds the shear capacity of the corresponding region (termed the "nominal shear length") of the end plate (see Figure 12).

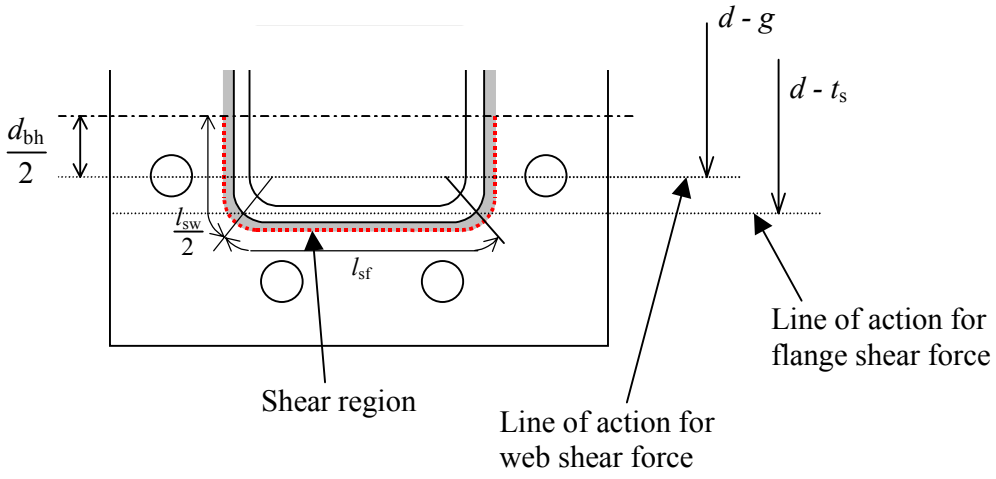

Figure 12. Punching shear failure modes

The *nominal shear length* is the length around the perimeter of the section that is assumed to fail as a result of the section pulling out from the end plate. This

length depends on the geometry of the connection as shown in Figure 12, and is divided into two regions, corresponding to flange failure and web failure. The flange failure length (l_{sf}) is defined as the length of the flat region on the section flange plus half the corners on either side.

$$l_{sf} = d - 5 \cdot t_s + \frac{\pi}{2} \cdot \left(2.5 \cdot t_s + s - \frac{t_p}{2} \right) \tag{30}$$

In the above equation, s denotes the weld leg length and it has been assumed that the external corner radius of the tubular section is 2.5 times the wall thickness. The shear force generated adjacent to the flange region is assumed to act through the centreline of the flange ($d - t_s$).

The web failure length (l_{sw}) considers the restraining effect of the bolts on the end plate. The assumed web failure length (l_{sw}) is shown in Figure 12 and is given by

$$l_{sw} = 2 \cdot \left(g - 2.5 \cdot t_s + \frac{d_{bh}}{2} + \frac{\pi}{4} \cdot \left(2.5 \cdot t_s + s - \frac{t_p}{2} \right) \right) \tag{31}$$

where d_{bh} is the diameter of the bolt head. The shear forces generated adjacent to the webs of the section are assumed to act at the level of the tensile bolts positioned beside the section webs ($d - g$).

To compare the theoretical data with the experimental data, the end plate design stress (f_p) defined in Equation 9 is used to define the end plate design stress in shear.

$$f_{\tau p} = \frac{f_p}{\sqrt{3}} \tag{32}$$

with respect to the Von Mises yield criterion.

The design moment of the connection with respect to punching shear is expressed as

$$M_{PS} = f_{\tau p} \cdot t_p \cdot \left[l_{sf} \cdot (d - t_s) + l_{sw} \cdot (d - g) \right] \tag{33}$$

where t_p is the end plate thickness, d is the section depth, and t_s is the section thickness.

Using Equations 30 to 33, the punching shear failure loads for the 10 eight-bolt tests have been calculated and are given in Table 7. The relevant geometrical and material properties are given in Tables 1 and 2, respectively.

Further comments on the appropriateness and accuracy of the punching shear model are provided in the next section, where all of the possible failure modes are compared with the test results.

Generalised Connection Model

The cumulative modified stub-tee method identifies two modes of connection failure, which are bolt capacity and end plate capacity. Bolt capacity (which may occur in conjunction with thick or intermediate plate behaviour) occurs when the tensile bolts fracture, while plate capacity (thin plate behaviour) occurs when a plastic mechanism forms in the end plate without deformation of the bolts. The plate capacity is independent of the bolt loads. Other failure modes not considered in the modified stub-tee analysis but which may occur in practice include shear failure of the end plate (punching shear) and plastic section failure. The generalised connection model presented in this section, the results of which are summarised in Table 7, considers each these failure modes and defines the ultimate capacity of the connection according to the critical mode.

The results shown in Table 7 indicate that although a total of ten eight-bolt tests were performed, four of these were limited in strength by punching shear failure and a further four were governed by plastic section capacity. Only two tests were governed by failure of the end plate itself, as computed using the stub tee analysis. Furthermore, both of the tests governed by end plate failure (Test #3 and #8) were limited by bolt capacity in conjunction with intermediate plate behaviour. Thin plate behaviour was not observed in any of the tests, and the thick end plate capacity was always preceded by the section capacity.

It can be seen in Table 7 that there is an excellent correspondence between the experimental and theoretical results, both in terms of the predicted failure mode and the numerical value. In only two instances (Tests #7 and #8) was the incorrect failure mode inferred, but even in these cases the predicted to test ratios of 0.97 (Test#7) and 0.93 (Test #8) are extremely good. The failure criteria and failure loads for the standard SHS tests (Tests #1, #3, and #4) and standard RHS tests (Tests #2, #5, #6) are presented in Figures 13 and 14,

respectively. In these figures, the three modes of failure discussed previously are shown. These modes are plastic section capacity (which is independent of the end plate thickness), the cumulative modified stub-tee capacity, and punching shear capacity.

Table 7. Connection Capacities

Test #	Experimental Moment M_{cu} (kNm)	Stub Tee Capacity M_{cpred} (kNm)	Punching Shear Capacity M_{PS} (kNm)	Theoretical Section Capacity M_s (kNm)	Ratio M_{pred} / M_u
1	116.0 (s)	117.8	126.6	116.3	1.00
2	124.5 (p)	164.1	116.8	128.4	1.07
3	93.9 (y)	92.8	94.9	116.3	1.01
4	116.0 (s)	124.9	156.0	116.3	1.00
5	92.7 (p)	127.4	87.6	128.4	1.06
6	136.7 (s)	173.4	146.0	128.4	1.06
7	113.2 (y)	119.2	134.7	116.3	0.97
8	97.6 (p)	104.9	123.1	116.3	0.93
9	133.0 (p)	172.8	123.2	128.4	1.08
10	119.0 (p)	143.2	110.0	128.4	1.08
				Mean	1.03
				Standard Dev.	0.05

(p) Punching shear failure observed
(s) Section capacity failure observed
(y) Failure by yield line formation and bolt fracture

The failure criteria for the SHS (Figure 13) demonstrates that for the given end plate details, an end plate thicker than 16 mm will result in plastic section failure, while an end plate thinner than 12 mm forms a mechanism (thin plate behaviour). Punching shear failure never governs for the square hollow section connections.

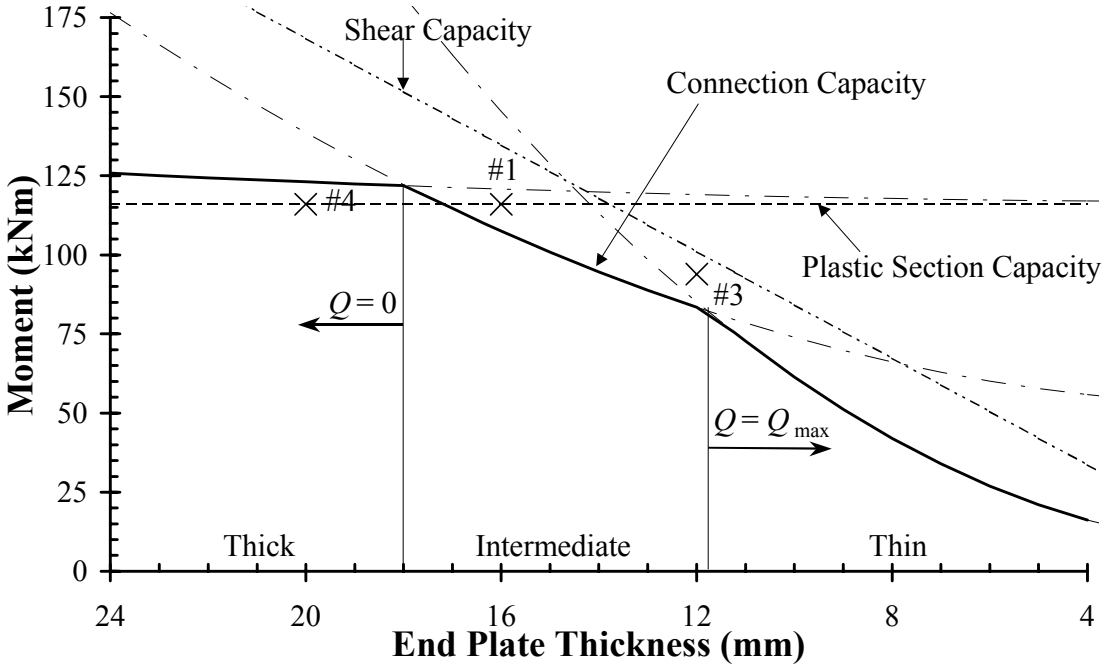

Figure 13. Failure criteria for SHS connections (s_o = 35 mm)

For rectangular hollow sections, the different depth-to-width aspect ratio results in punching shear failure dominating (Figure 14). Connections containing end plates thicker than 17 mm will attain full plastic section capacity, while end plates thinner than 9 mm will fail as a result of a plastic mechanism forming in the end plate (thin plate behaviour). Connections containing end plates thinner than 17 mm and thicker than 9 mm fail as a result of punching shear.

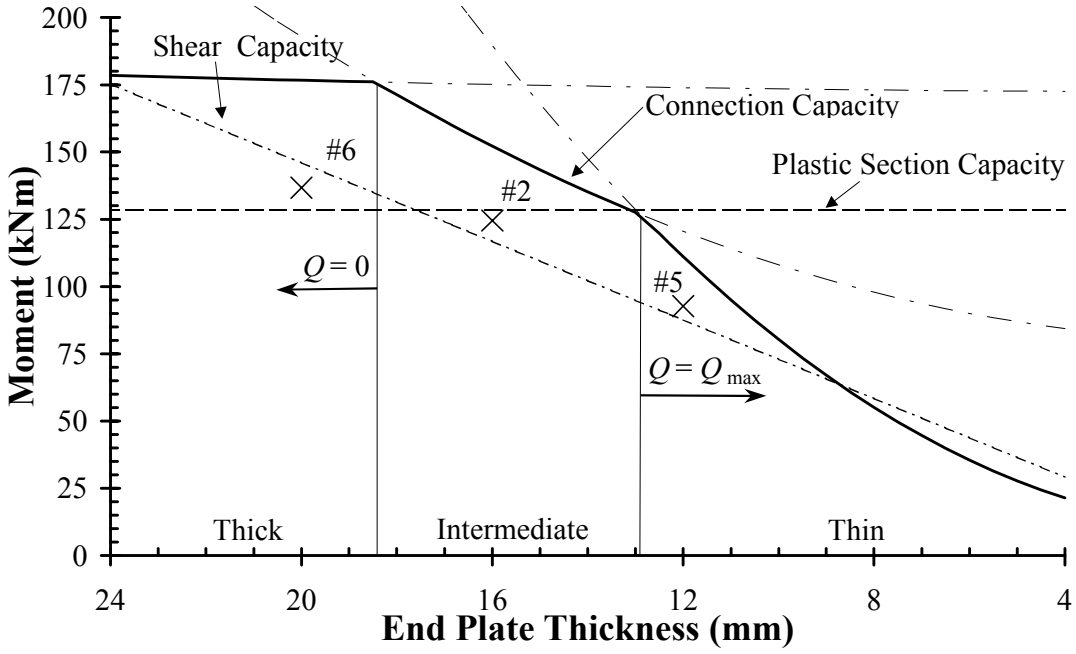

Figure 14. Failure criteria for RHS connections (s_o = 35 mm)

Conclusions

In this paper, design models are presented for prediction of the strength and behaviour of eight-bolt moment end plate connections joining square and rectangular hollow sections. The models consider a variety of failure modes including the formation of a plastic collapse mechanism in the end plate, tensile failure of the bolts, plastic section failure in the connected beam, and punching shear (tear out) failure. Plastic mechanism analysis comprising complex two-dimensional patterns of yield lines is employed for the investigation of end plate failure modes, and a modified version of stub tee analysis provides the means through which the effects of prying forces are incorporated in the model. The stub tee analysis is termed the "cumulative modified stub tee model" since it considers prying effects independently in the "Vertical Beam" and "Horizontal Beam" bending directions for the end plate.

In comparison with the four-bolt end plate connections considered in an earlier paper (Wheeler et al., 1998), the eight-bolt connections are stiffer and stronger for an equivalent end plate thickness. The experimental and analytical results indicate that for the SHS connections, plastic section capacity failure dominates with end plate failure occurring only for the most flexible end plate configurations. For the RHS connections, the failure mode is predominantly that of punching shear, with plastic section capacity limiting the strength for the thicker end plates. The transition between the different failure modes which occurs with changing end plate thickness is captured very well by the analytical model. The model demonstrates excellent correlation with the test results with an overall mean predicted to experimental ratio of 1.03 and a standard deviation of 0.05. The model is effective in its consideration of all relevant failure modes which can occur including plastic mechanism formation in the end plate, bolt fracture, plastic section failure and punching shear failure.

The models developed in this report are based on the experimental results for ten (10) connections. To verify the model and define appropriate limits additional experimental or numerical studies are required. Studies to verify the assumptions regarding the shear capacity of the connections also require verification.

References

Agerskov, H., (1976), "High-Strength Bolted Connections Subject to Prying", *Journal of Structural Division*, ASCE, **102**(1), 161-175.

AISC (1990), *Hollow Structural Sections Connections Manual*, American Institute of Steel Construction, Inc.

Kato, B. and McGuire, W. (1973). "Analysis of T-Stub Flange-to-Column Connections", *Journal of Structural Division*, ASCE, **99**(5), pp 865-888.

Kato, B. and Mukai, A. (1985). "Bolted Tension Flanges Joining Square Hollow Section Members", *Journal of Construction Steel Research*, **5**, 163-177.

Kato, B. and Mukai, A. (1991). "High Strength Bolted Flanges Joints of SHS Stainless Steel Columns", Proceedings International Conference on Steel and Aluminium Structures, Singapore, May 1991.

Kennedy, N. A., Vinnakota, S. and Sherbourne A. N., (1981). "The Split-Tee Analogy in Bolted Splices and Beam-Column Connections", Joints in Structural Steelwork, John Wiley &sons, London-Toronto, 1981, pp. 2.138-2.157.

Nair, R. S., Birkemoe, P. C. and Munse, W. H., (1974). "High Strength Bolts Subject to Tension and Prying", *Journal of the Structural Division*, ASCE, **100**(2), pp 351-372.

Packer, J. A., Bruno, L., Birkemoe, P. C. (1989). "Limit Analysis of Bolted RHS Flange Plate Joints" *Journal of Structural Engineering*, ASCE, **115**(9), 2226-2241.

SA (1981a), *AS 1252-1981: High-strength Steel Structural Bolts with Associated Nuts and Washers for Structural Engineering*, Standards Australia, Sydney.

SA (1981b), *AS 3678-1981: Structural Steel – Hot-rolled plates, floorplates and slabs*, Standards Australia, Sydney.

SA (1990), *AS 4100-1990: Steel Structures*, Standards Australia, Sydney.

SA (1991a), *AS 1163-1981: Structural Steel Hollow Sections*, Standards Australia, Sydney.

SA (1991b). *AS 1554.1-1991: Structural Steel Welding - Part 1: Welding of Steel Structures*, Standards Australia, Sydney.

Syam, A. A. & Chapman, B. G., (1996), *Design of Structural Steel Hollow Section Connections. Volume 1: Design Models*, 1st Edition, Australian Institute of Steel Construction, Sydney.

Wheeler, A. T., Clarke, M. J. and Hancock, G. J. (1995). "Tests of Bolted Flange Plate Connections Joining Square and Rectangular Hollow Sections", Proceedings, Fourth Pacific Structural Steel Conference, Singapore, 97–104.

Wheeler A. T., Clarke M. J. and Hancock G. J., (1997), "Bending Tests of Bolted End Plate Connections in Cold Formed Rectangular Hollow Sections", *Research Report*, No. R736, Department of Civil Engineering, The University of Sydney.

Wheeler A. T., Clarke M. J., Hancock G. J. and Murray, T. M. (1998). "Design Model for Bolted Moment End Plate Connections Joining Rectangular Hollow Sections", Journal of Structural Engineering, ASCE, 124(2), 164–173.

Wheeler, A. T. (1998). "The Behaviour of Bolted Moment End Plate Connections in Rectangular Hollow Sections Subjected to Flexure", PhD Thesis, Department of Civil Engineering, The University of Sydney.

Appendix A. Yield Line Analysis

A.1 General

In the following development, it is assumed that the plastic collapse mechanisms may form either through failure of the end plate, failure of the tensile bolts or a combination of both. The moment at which a plastic collapse mechanism forms is determined using virtual work principles. The virtual internal work (U_I) and virtual external work (U_E) are calculated by applying a virtual displacement (δ) to the tensile flange of the connection and then determining the (compatible) induced virtual displacements elsewhere in the connection. The internal work (U_I) is the sum of the work generated through the formation of plastic yield lines (U_p) and yielding of the bolts (U_b),

$$U_I = U_p + U_b \tag{A.1}$$

The internal work generated through the formation of yield lines in the end plate is expressed as

$$U_p = \left(\sum \theta_{uv} \cdot \ell_{uv}\right) \cdot m_p \tag{A.2}$$

where m_p is the full plastic moment of the end plate per unit length, θ_{uv} is the rotation undergone by the yield line uv (formed between the planes u and v), and l_{uv} is the length of the corresponding yield line.

The angle (θ_{uv}) between two planes u and v is determined using vector analysis. Assuming small angles

$$\theta_{uv} = \frac{\boldsymbol{n}_u \times \boldsymbol{n}_v}{\boldsymbol{n}_u \bullet \boldsymbol{n}_v}$$

with the x and y components given by

$$\begin{aligned} \theta_{xuv} &= \frac{(\boldsymbol{n}_u \times \boldsymbol{n}_v) \bullet \boldsymbol{i}}{\boldsymbol{n}_u \bullet \boldsymbol{n}_v} \\ \theta_{yuv} &= \frac{(\boldsymbol{n}_u \times \boldsymbol{n}_v) \bullet \boldsymbol{j}}{\boldsymbol{n}_u \bullet \boldsymbol{n}_v} \end{aligned} \tag{A.3}$$

where $\boldsymbol{n}_u$ and $\boldsymbol{n}_v$ are vectors normal to the planes u and v, respectively.

As the yield line patterns that develop in the eight-bolt connections are often complex, the analysis may be simplified by expressing the yield line rotations and lengths in terms of the *x* and *y* components. The work generated in the end plate is expressed component-wise as

$$U_{\mathrm{p}} = \left(\sum \theta_{xuv} \cdot \ell_{xuv} + \sum \theta_{yuv} \cdot \ell_{yuv}\right) \cdot m_{\mathrm{p}} \tag{A.4}$$

where l_{xuv} and l_{yuv} are the projections of the yield line *uv* onto the *x* and *y* axes, respectively, and the rotations θ_{xuv} and θ_{yuv} are correspondingly defined.

The internal work generated by the bolts is defined as the product of the imposed virtual displacement of the bolt ($\delta_{\mathrm{b}i}$), and the yield load of the bolt ($B_{\mathrm{y1}i}$).

$$U_{\mathrm{b}} = \sum B_{\mathrm{y1}i} \cdot \delta_{\mathrm{b}i} \tag{A.5}$$

Similarly, the external work is defined in terms of the applied moment as

$$U_{\mathrm{E}} = M_{\mathrm{yl}} \cdot \frac{\delta}{d} \tag{A.6}$$

The applied moment to cause plastic collapse of the connection (M_{y1}) is now determined by equating the external work (Equation A.6) and the internal work (sum of Equations A.4 and A.5).

As yield line analysis produces upper bound solutions, seven different plastic collapse mechanisms for the eight-bolt connection are identified and analysed in this appendix to determine the actual plastic collapse moment. All the yield line mechanisms described in this appendix contain a vertical axis of symmetry, which is used to simplify the theoretical analysis. For the first two mechanisms presented (Mechanism 1 and 2), the internal work of the connection is a result of plastic deformation in the end plate only. Mechanisms 3 to 6 involve both the development of yield lines in the end plate, and yielding of the bolts. The final plastic collapse mechanism (Mechanism 7) is solely a function of yielding in the bolts, with no yielding occurring in the end plate.

A.2 Mechanism 1

Mechanism 1, shown in Figure A.1, consists of eight yield lines. The yield lines *12*, *23* and *24*, form at the interface of the beam section and the end plate. Yield lines *35* and *45* are located between the tensile corner of the section and bolt holes #3 and #4, as shown. The remaining three yield lines (*14*, *15* and *13*) are defined by the intersection of Plane 1 with Planes 4, 3 and 5 respectively.

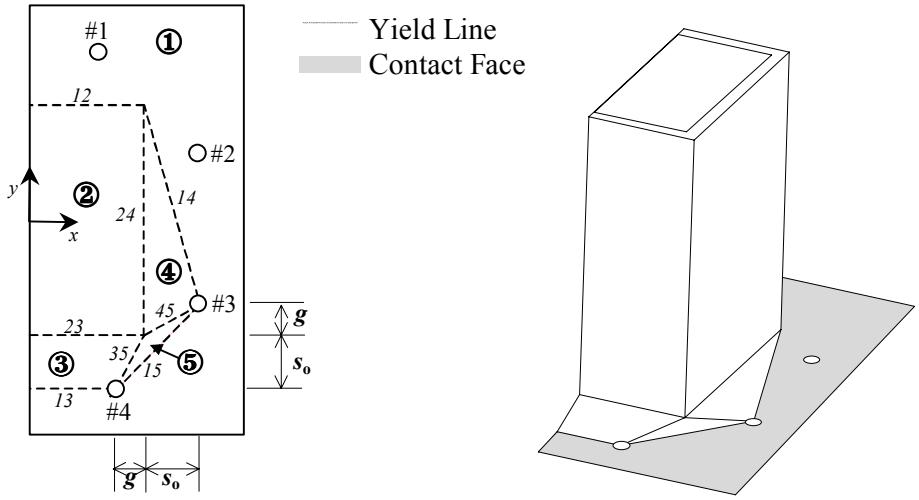

Figure A.1. Mechanism 1

Applying the virtual displacement (δ) at the bottom of the section (i.e. along yield line *23*), the displaced configuration of Planes 1 through to 5 can be expressed in terms of their normal vectors as follows:

$$\boldsymbol{n}_2 = 0\,\mathbf{i} + \delta\,\mathbf{j} + d\,\mathbf{k}$$
$$\boldsymbol{n}_3 = 0\,\mathbf{i} - \delta\,\mathbf{j} + s_o\,\mathbf{k}$$
$$\boldsymbol{n}_4 = (d-g)\cdot\delta\,\mathbf{i} + s_o\cdot\delta\,\mathbf{j} + d\cdot s_o\,\mathbf{k}$$
$$\boldsymbol{n}_5 = \delta\,\mathbf{i} + -\delta\,\mathbf{j} + (s_o - g)\,\mathbf{k}$$

Using Equation A.3, the resulting angles between the intersecting planes are calculated and given in Table A.1. Also presented in this table are the lengths of the yield lines and the resulting internal work generated by each yield line.

Table A.1. Internal Virtual Work Details for Plastic Collapse Mechanism 1

4	θ_{xuv}	θ_{yuv}	ℓ_{xuv}	ℓ_{yuv}	U_{puv}
12	$\frac{\delta}{d}$	0	$\frac{b}{2}$	0	$\frac{b\cdot\delta}{2\cdot d}\cdot m_p$
13	$\frac{\delta}{s_o}$	0	$\frac{b}{2}-g$	0	$\frac{(b-2\cdot g)\cdot\delta}{2\cdot s_o}\cdot m_p$
14	$\frac{\delta}{d}$	$\frac{\delta\cdot(d-g)}{d\cdot s_o}$	s_o	$d-g$	$\frac{\left(s_o^2+(d-g)^2\right)\cdot\delta}{s_o\cdot d}\cdot m_p$
15	$\frac{\delta}{s_o-g}$	$\frac{\delta}{s_o-g}$	$g+s_o$	$g+s_o$	$2\cdot\frac{(g+s_o)\cdot\delta}{s_o-g}\cdot m_p$
23	$\frac{\delta\cdot(d+s_o)}{d\cdot s_o}$	0	$\frac{b}{2}$	0	$\frac{(d+s_o)\cdot b\cdot\delta}{2\cdot d\cdot s_o}\cdot m_p$
24	0	$\frac{\delta\cdot(d-g)}{d\cdot s_o}$	0	d	$\frac{(d-g)\cdot\delta}{s_o}\cdot m_p$
35	$\frac{\delta\cdot g}{s_o\cdot(s_o-g)}$	$\frac{\delta}{(s_o-g)}$	g	s_o	$\frac{\left(s_o{}^2+g^2\right)\cdot\delta}{s_o\cdot(s_o-g)}\cdot m_p$
45	$\frac{\delta\cdot(s_o+d-g)}{d\cdot(s_o-g)}$	$\frac{\delta\cdot(s_o+d-g)\cdot g}{s_o\cdot d\cdot(s_o-g)}$	s_o	g	$\frac{(s_o+d-g)\cdot\left(s_o^2+g^2\right)\cdot\delta}{s_o\cdot d\cdot(s_o-g)}\cdot m_p$

Summing the internal work (U_p) in the end plate (from Table A.1) and equating it to the external work (Equation A.6) enables the moment at which plastic collapse occurs according to Mechanism 1 to be expressed as

$$M_{yl}=2\left(\frac{2\cdot d^2-4\cdot d\cdot g+g^2+s_o{}^2+(s_o+d)\cdot b}{d\cdot s_o}+2\frac{g+s_o}{s_o-g}+\frac{(s_o-g+2\cdot d)\cdot\left(g^2+s_o{}^2\right)}{s_o\cdot d\cdot(s_o-g)}\right)\cdot d\cdot m_p \qquad (A.7)$$

The validity of this mechanism is limited by the fact that the bolt position dimensions g and s_o must satisfy $g\le s_o$ since otherwise yield line *15* cannot form.

A.3 Mechanism 2

Mechanism 2, shown in Figure A.2, consists of ten yield lines and assumes the bolts do not yield. The various planes and yield lines are defined in Figure A.2. The mechanism is defined by an imposed virtual displacement of δ at the tensile flange of the section (yield line *23*). Also, the bottom corner of the end plate is assumed to displace vertically by an amount $k\delta$ with the value for k determined by minimising the resulting expression for the plastic collapse moment of the connection.

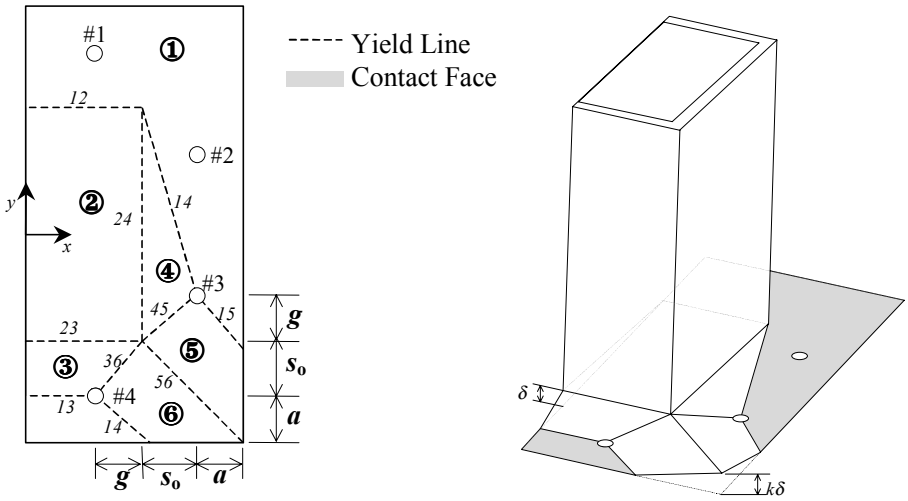

Figure A.2. Mechanism 2

For imposed virtual displacements of δ at the tensile flange and $k\delta$ at the tensile corner, planes 1 to 6 can be expressed in terms of their respective normal vectors as

$$\boldsymbol{n}_1 = 0\,\mathbf{i} + 0\,\mathbf{j} + \mathbf{k}$$
$$\boldsymbol{n}_2 = 0\,\mathbf{i} + \delta\,\mathbf{j} + d\,\mathbf{k}$$
$$\boldsymbol{n}_3 = 0\,\mathbf{i} - \delta\,\mathbf{j} + s_o\,\mathbf{k}$$
$$\boldsymbol{n}_4 = (d-g)\cdot\delta\,\mathbf{i} + s_o\cdot\delta\,\mathbf{j} + d\cdot s_o\,\mathbf{k}$$
$$\boldsymbol{n}_5 = (s_o + a + g\cdot(1-k))\cdot\delta\,\mathbf{i} + (k\cdot s_o + a)\cdot\delta\,\mathbf{j} + (s_o + g)\cdot(s_o + a)\mathbf{k}$$
$$\boldsymbol{n}_6 = -(k\cdot s_o + a)\cdot\delta\,\mathbf{i} - (s_o + a + g\cdot(1-k))\cdot\delta\,\mathbf{j} + (s_o + a)\cdot(s_o + g)\,\mathbf{k}$$

The rotation of the yield lines with respect to the *x* and *y* axes are found using Equation A.3 and are presented in Table A.2a. The respective yield line lengths and internal work for each yield line are given in Table A.2b.

Table A.2a. Virtual Rotations of Yield Lines for Mechanism 2

uv	θ_{xuv}	θ_{yuv}
12	$\frac{\delta}{d}$	0
13	$\frac{\delta}{d}$	$\frac{\delta\cdot(d-g)}{d\cdot s_o}$
14	$\frac{(k\cdot s_o+a)\cdot\delta}{(s_o+g)\cdot(s_o+g)}$	$\frac{(s_o+a+g-k\cdot g)\cdot\delta}{(s_o+g)\cdot(s_o+g)}$
15	$\frac{(s_o+a+g-k\cdot g)\cdot\delta}{(s_o+g)\cdot(s_o+g)}$	$\frac{(k\cdot s_o+a)\cdot\delta}{(s_o+g)\cdot(s_o+g)}$
16	$\frac{\delta}{s_o}$	0
23	$\frac{\delta\cdot(d-s_o)}{d\cdot s_o}$	0
24	0	$\frac{\delta\cdot(d-g)}{d\cdot s_o}$
26	$\frac{(2\cdot s_o\cdot(g+s_o+a)+g\cdot(a-k\cdot s_o))\cdot\delta}{s_o\cdot(s_o+g)\cdot(s_o+a)}$	$\frac{(k\cdot s_o+a)\cdot\delta}{(s_o+g)\cdot(s_o+a)}$
45	$\frac{((s_o+g)(s_o+a)-d\cdot(k\cdot s_o+a))\cdot\delta}{d\cdot(s_o+g)\cdot(s_o+a)}$	$\frac{((s_o+g)(s_o+a)-d\cdot(k\cdot s_o+a))\cdot g\cdot\delta}{d\cdot(s_o+g)\cdot(s_o+a)\cdot s_o}$
56	$\frac{(g+s_o+2\cdot a+(s_o-g)\cdot k)\cdot\delta}{(s_o+a)\cdot(s_o+g)}$	$\frac{(g+s_o+2\cdot a+(s_o-g)\cdot k)\cdot\delta}{(s_o+a)\cdot(s_o+g)}$

Table A.2b. Yield Line Lengths and Virtual Internal Work for Mechanism 2

i	ℓ_{xi}	ℓ_{yi}	U_{pi}
12	$\frac{b}{2}$	0	$\frac{b\cdot\delta}{2\cdot d}\cdot m_p$
13	$\frac{b}{2}-g$	0	$\frac{(b-2\cdot g)\cdot\delta}{2\cdot s_o}\cdot m_p$
14	s_o	$d-g$	$\frac{\left(s_o^{\,2}+(d-g)^2\right)\cdot\delta}{d\cdot s_o}\cdot m_p$
15	a	$\frac{(g+s_o+a-k\cdot g)\cdot a}{k\cdot s_o+a}$	$\frac{a\cdot\left((s_o+a+g-k\cdot g)^2+(k\cdot s_o+a)^2\right)\cdot\delta}{(s_o+g)\cdot(s_o+g)\cdot(k\cdot s_o+a)}\cdot m_p$
16	$\frac{(g+s_o+a-k\cdot g)\cdot a}{k\cdot s_o+a}$	a	$\frac{a\cdot\left((s_o+a+g-k\cdot g)^2+(k\cdot s_o+a)^2\right)\cdot\delta}{(s_o+g)\cdot(s_o+g)\cdot(k\cdot s_o+a)}\cdot m_p$
23	$\frac{b}{2}$	0	$\frac{(d+s_o)\cdot b\cdot\delta}{2\cdot d\cdot s_o}\cdot m_p$
24	0	d	$\frac{\delta\cdot(d-g)}{s_o}\cdot m_p$
36	g	s_o	$\frac{\left(g^2+s_o^{\,2}\right)\cdot(k\cdot s_o+a)\cdot\delta}{s_o\cdot(s_o+g)\cdot(s_o+a)}\cdot m_p$
45	s_o	g	$\frac{((s_o+g)(s_o+a)-d\cdot(k\cdot s_o+a))\cdot\left(s_o^2+g^2\right)\cdot\delta}{s_o\cdot d\cdot(s_o+g)\cdot(s_o+a)}\cdot m_p$
56	s_o+a	s_o+a	$2\cdot\frac{(g+s_o+2\cdot a+(s_o-g)\cdot k)\cdot\delta}{(s_o+g)}\cdot m_p$

The moment to cause plastic collapse according to Mechanism 2 is found by summing the internal work (U_p) in Table A.2b and equating it to the external work (Equation A.6). The resulting expression for the plastic collapse moment is

$$M_{yl} = 2 \cdot \left[\begin{array}{l} \dfrac{b \cdot (s_o + b) + {s_o}^2 + 2 \cdot (d-g)^2 - g^2}{s_o \cdot d} + \dfrac{(k \cdot s_o + a) \cdot \left({s_o}^2 + g^2 + 2 \cdot a \cdot s_o\right)}{s_o \cdot (g + s_o) \cdot (s_o + a)} \\ + \dfrac{2 \cdot (s_o + a + g \cdot (1-k)) \cdot s_o \cdot a + (k \cdot s_o + a)^2 \cdot \left(g^2 + {s_o}^2\right)}{s_o \cdot (g + s_o) \cdot (s_o + a) \cdot (k \cdot s_o + a)} \\ + 4 \cdot \dfrac{2 \cdot a + g \cdot (1-k) + s_o \cdot (1+k)}{g + s_o} \end{array} \right] \cdot d \cdot m_p \qquad \text{(A.8)}$$

The governing failure moment is determined by minimising the above equation with respect to k, with $k \geq 0$. This minimisation is performed numerically in the present work.

A.4 Mechanism 3

Mechanism 3, shown in Figure A.3, consists of eight yield lines coupled with yielding of the bolts at position #4. As in Mechanism 2, a displacement of δ is imposed on the tensile flange of the section generating the yield lines as shown. It is assumed that this displacement causes the bottom right corner of the end plate to displace vertically by an amount $k\delta$.

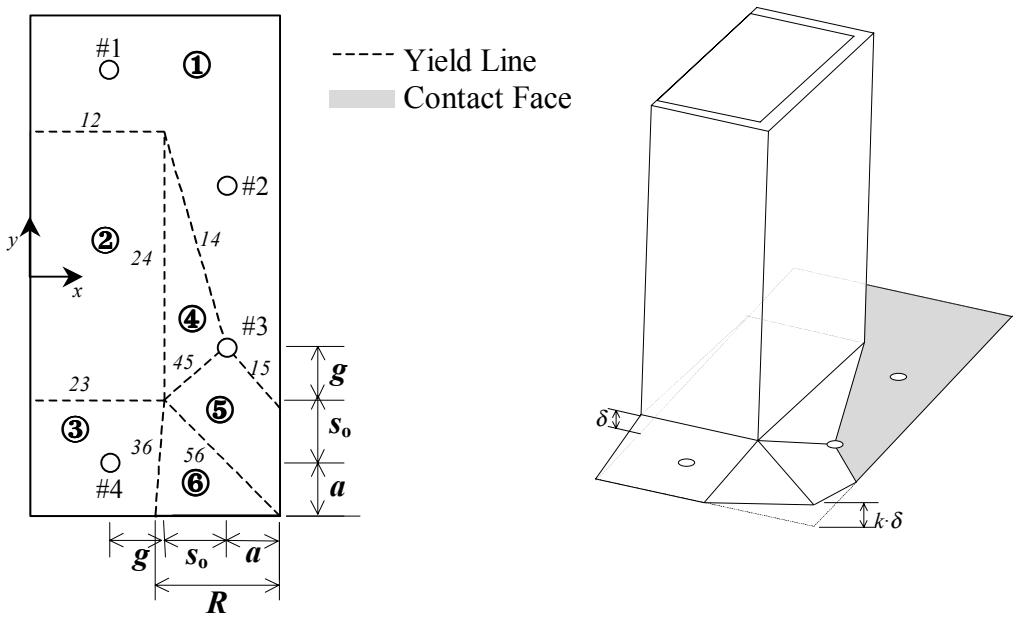

Figure A.3. Mechanism 3

For the given imposed virtual displacements, Planes 1 to 6 can be expressed in terms of their respective normal vectors as

$$\boldsymbol{n}_1 = 0\,\mathbf{i} + 0\,\mathbf{j} + \mathbf{k}$$
$$\boldsymbol{n}_2 = 0\,\mathbf{i} + \delta\,\mathbf{j} + d\,\mathbf{k}$$
$$\boldsymbol{n}_3 = 0\,\mathbf{i} - \delta\,\mathbf{j} + (s_o + a)\,\mathbf{k}$$
$$\boldsymbol{n}_4 = (d - g)\cdot\delta\,\mathbf{i} + s_o\cdot\delta\,\mathbf{j} + d\cdot s_o\,\mathbf{k}$$
$$\boldsymbol{n}_5 = (s_o + a + g - k\cdot g)\cdot\delta\,\mathbf{i} + (s_o\cdot k + a)\cdot\delta\,\mathbf{j} + (g + s_o)\cdot(s_o + a)\,\mathbf{k}$$
$$\boldsymbol{n}_6 = -k\cdot(s_o + a)\cdot\delta\,\mathbf{i} + -(k\cdot(s_o + a - R) + R)\cdot\delta\,\mathbf{j} + R\cdot(s_o + a)\,\mathbf{k}$$

The rotations of the yield line with respect to the *x* and *y* axes are given in Table A.3a . The respective yield lines lengths, and the corresponding internal work generated by each yield line, are given in Table A.3b.

Table A.3a. Virtual Rotations of Yield Lines for Mechanism 3

uv	θ_{xuv}	θ_{yuv}
12	$\frac{\delta}{d}$	0
14	$\frac{\delta}{d}$	$\frac{\delta\cdot(d-g)}{d\cdot s_o}$
15	$\frac{(k\cdot s_o+a)\cdot\delta}{(s_o+g)\cdot(s_o+g)}$	$\frac{(s_o+a+g-k\cdot g)\cdot\delta}{(s_o+g)\cdot(s_o+a)}$
23	$\frac{\delta\cdot(d+s_o+a)}{d\cdot(s_o+a)}$	0
24	0	$\frac{\delta\cdot(d-g)}{d\cdot s_o}$
35	$\frac{(s_o+g+a)\cdot\delta}{(s_o+a)\cdot(s_o+g)}$	$\frac{(s_o+g+a)\cdot\delta}{(s_o+a)\cdot(s_o+g)}$
36	$\frac{k\cdot(a+s_o-R)\cdot\delta}{(s_o+g)\cdot R}$	$\frac{k\cdot\delta}{R}$
45	$\frac{(d\cdot(a+s_o\cdot k)-(s_o+g)(s_o+a))\cdot\delta}{d\cdot(s_o+g)\cdot(s_o+a)}$	$\frac{g\cdot(d\cdot(a+s_o\cdot k)-(s_o+g)(s_o+a))\cdot\delta}{d\cdot(s_o+g)\cdot(s_o+a)\cdot s_o}$
56	$\frac{((g+s_o+a)\cdot(s_o\cdot k+R)+g\cdot k\cdot(a-R))\cdot\delta}{(s_o+a)\cdot(s_o+g)\cdot R}$	$\frac{((g+s_o+a)\cdot(s_o\cdot k+R)+g\cdot k\cdot(a-R))\cdot\delta}{(s_o+a)\cdot(s_o+g)\cdot R}$

Notes If $k > 0$, terms relating to yield line *35* are irrelevant

If $k = 0$, terms relating to yield lines *56* and *36* are irrelevant

Table A.3b. Yield Line Lengths and Virtual Internal Work for Mechanism 3

uv	ℓ_{xuv}	ℓ_{yuv}	U_{puv}
12	$\frac{b}{2}$	0	$\frac{b\cdot\delta}{2\cdot d}\cdot m_p$
14	s_o	$d-g$	$\frac{\left(s_o^2+(d-g)^2\right)\cdot\delta}{d\cdot s_o}\cdot m_p$
15	a	$\frac{(g+s_o+a-k\cdot g)\cdot a}{k\cdot s_o+a}$	$\frac{\left((a+s_o\cdot k)^2+(s_o+a+g-k\cdot g)\right)^2\cdot\delta}{(s_o+g)\cdot(s_o+a)\cdot(a+s_o\cdot k)}\cdot m_p$
23	$\frac{b}{2}$	0	$\frac{(a+s_o+d)\cdot b\cdot\delta}{2\cdot d\cdot(s_o+a)}\cdot m_p$
24	0	d	$\frac{(d-g)\cdot\delta}{s_o}\cdot m_p$
35	s_o+a	s_o+a	$2\cdot\frac{(s_o+g+a)\cdot\delta}{(s_o+g)}\cdot m_p$
36	$a+s_o-R$	s_o+a	$\frac{k\cdot\left((a+s_o-R)^2+(s_o+a)^2\right)\cdot\delta}{(s_o+a)\cdot R}\cdot m_p$
45	s_o	g	$\frac{((s_o+g)\cdot(s_o+a)-d\cdot(s_o\cdot k+a))\cdot\left(s_o{}^2+g^2\right)\cdot\delta}{(s_o+g)\cdot(s_o+a)\cdot s_o\cdot d}\cdot m_p$
56	s_o+a	s_o+a	$2\cdot\frac{((g+s_o+a)\cdot(s_o\cdot k+R)+g\cdot k\cdot(a-R))\cdot\delta}{(s_o+g)\cdot R}\cdot m_p$

Notes If $k > 0$, terms relating to yield line *35* are irrelevant

If $k = 0$, terms relating to yield lines *56* and *36* are irrelevant

To allow the formation of Mechanism 3, the bolt at position #4 (Figure A.3) yields and hence generates additional internal work (U_b). This internal work is the product of the virtual displacement imposed to the bolt, and the bolt yield load.

$$U_{b4}=\frac{a\cdot\delta}{s_o+a}\cdot B_{y1} \tag{A.9}$$

The resulting moment to cause Mechanism 3 is determined by equating the internal and external work. The total internal work (U_I) is found by summing the internal work in the end plate (Table A.3b) and the internal work done by the bolts (U_b).

$$M_{\text{yl}} = 2 \cdot \left(U_{\text{p12}} + U_{\text{p}_{14}} + U_{\text{p15}} + U_{\text{p23}} + U_{\text{p24}} + U_{\text{p36}} + U_{\text{p45}} + U_{\text{p56}} + U_{\text{b4}}\right) \cdot \frac{d}{\delta} \qquad \text{(A.10)}$$

For the unique case when $k = 0$, yield lines *56* and *36* are replaced by a single yield line *35* and the resulting work is defined as

$$M_{\text{yl}} = 2 \cdot \left(U_{\text{p}12} + U_{\text{p}14} + U_{\text{p}15} + U_{\text{p}23} + U_{\text{p}24} + U_{\text{p}35} + U_{\text{p}45} + U_{\text{b4}}\right) \cdot \frac{d}{\delta} \qquad \text{(A.11)}$$

When $k > 0$ the minimum value for M_{yl} is obtained by minimising Equation A.11 with respect to k and R, where R is the horizontal distance from the end plate corner to yield line *46*. For the mechanism to form, the value of R must be greater than zero but less than $(s_\text{o} + a) \cdot g / s_\text{o}$.

A.5 Mechanism 4

Mechanism 4, shown in Figure A.4, consists of eight yield lines coupled with yielding of the bolts at positions #3 and #4. Yield line *15*, defined by the intersection of Planes 1 and 5, starts at bolt #2 and intersects the edge of the end plate at a distance *R* from the bottom right-hand corner. Yield line *56*, defined by Planes 5 and 6, starts at the tensile corner of the section and intersects the edge of the end plate at a distance of *R* from the bottom right-hand corner.

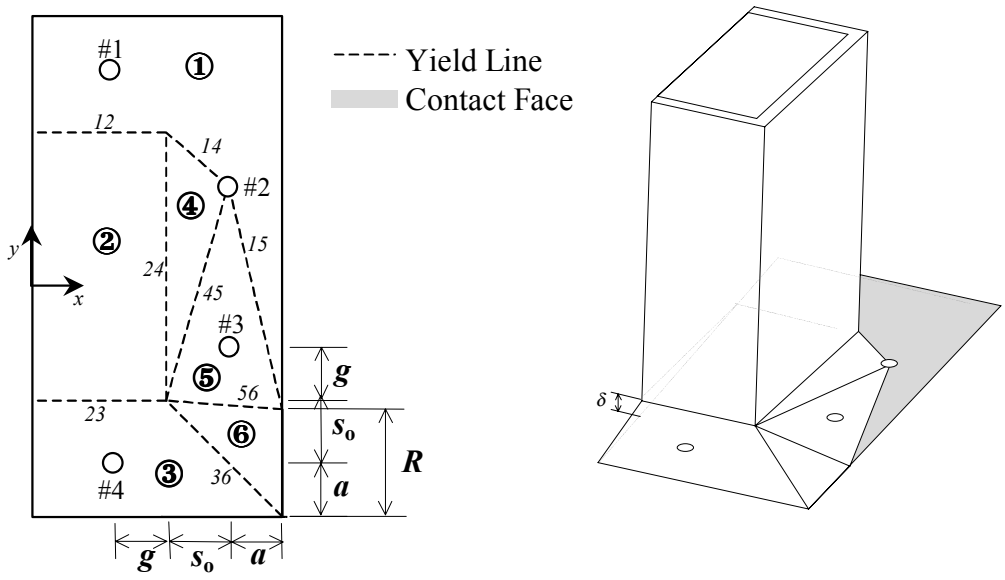

Figure A.4. Mechanism 4

For the given imposed virtual displacement at the tensile flange of the section, Planes 1 to 6 can be expressed in terms of their normal vectors as

$$\boldsymbol{n}_1 = 0\,\mathbf{i} + 0\,\mathbf{j} + \mathbf{k}$$
$$\boldsymbol{n}_2 = 0\,\mathbf{i} + \delta\,\mathbf{j} + d\,\mathbf{k}$$
$$\boldsymbol{n}_3 = 0\,\mathbf{i} - \delta\,\mathbf{j} + (s_o + a)\,\mathbf{k}$$
$$\boldsymbol{n}_4 = g\cdot\delta\,\mathbf{i} + s_o\cdot\delta\,\mathbf{j} + d\cdot s_o\,\mathbf{k}$$
$$\boldsymbol{n}_5 = (d - g + s_o + a - R)\cdot\delta\,\mathbf{i} + a\cdot\delta\,\mathbf{j} + (s_o + d - g)\cdot(s_o + a) - R\cdot s_o\,\mathbf{k}$$
$$\boldsymbol{n}_6 = R\cdot\delta\,\mathbf{i} + 0\,\mathbf{j} + R\cdot(s_o + a)\,\mathbf{k}$$

Using Equation A.3, the angles of rotation, undergone by each yield line in the *x* and *y* directions can be determined and are given in Table A.4a. The lengths of

the yield lines, in terms of their *x* and *y* components, and the total internal work for each yield line, are listed in Table A.4b.

Table A.4a. Virtual Rotations of Yield Lines for Mechanism 4

	θ_{xuv}	θ_{yuv}
12	$\frac{\delta}{d}$	0
14	$\frac{\delta}{d}$	$\frac{g\cdot\delta}{d\cdot s_o}$
15	$\frac{a\cdot\delta}{(s_o+d-g)\cdot(s_o+a)-R\cdot s_o}$	$\frac{(s_o+a+d-g-R)\cdot\delta}{(s_o+d-g)\cdot(s_o+a)-R\cdot s_o}$
23	$\frac{\delta\cdot(d+s_o+a)}{d\cdot(s_o+a)}$	0
24	0	$\frac{\delta\cdot g}{d\cdot s_o}$
36	$\frac{\delta}{(s_o+a)}$	$\frac{\delta}{(s_o+a)}$
45	$\frac{(d\cdot s_o+(s_o-g)(s_o+a)-R\cdot s_o)\cdot\delta}{((s_o+d-g)\cdot(s_o+a)-R\cdot s_o)\cdot d}$	$\frac{((s_o-g)(s_o+a)+(d-R)\cdot s_o)\cdot(d-g)\cdot\delta}{d\cdot((s_o+d-g)\cdot(s_o+a)-R\cdot s_o)\cdot s_o}$
56	$\frac{a\cdot\delta}{(s_o+d-g)\cdot(s_o+a)-R\cdot s_o}$	$\frac{a\cdot(s_o+a-R)\cdot\delta}{((s_o+a)\cdot(s_o+d-g)-R\cdot s_o)\cdot(s_o+a)}$

Table A.4b. Virtual Internal Work due to Bolts for Mechanism 4

	U_{bi}
3	$\frac{B_{y1}\cdot a\cdot(d-2\cdot g)\cdot\delta}{(s_o+a)\cdot(s_o+d-g)-R\cdot s_o}$
4	$\frac{B_{y1}\cdot a\cdot\delta}{s_o+a}$

Table A.4c. Yield Line Lengths and Virtual Internal Work for Mechanism 4

uvi	ℓ_{xuv}	ℓ_{yuv}	U_{puv}
12	$\frac{b}{2}$	0	$\frac{b\cdot\delta}{2\cdot d}\cdot m_p$
14	s_o	g	$\frac{(s_o^2+g^2)\cdot\delta}{d\cdot s_o}\cdot m_p$
15	a	$s_o+a+d-g-R$	$\frac{\left((s_o+a+d-g-R)^2+a^2\right)\cdot\delta}{(s_o+d-g)\cdot(s_o+a)-R\cdot s_o}\cdot m_p$
23	$\frac{b}{2}$	0	$\frac{(a+s_o+d)\cdot b\cdot\delta}{2\cdot d\cdot(s_o+a)}\cdot m_p$
24	0	d	$\frac{\delta\cdot g}{s_o}\cdot m_p$
36	s_o+a	s_o+a	$2\cdot\delta\cdot m_p$
45	s_o	$d-g$	$\frac{((s_o-g)(s_o+a)+(d-R)\cdot s_o)\cdot\left((d-g)^2+s_o^2\right)\cdot\delta}{d\cdot((s_o+d-g)\cdot(s_o+a)-R\cdot s_o)\cdot s_o}\cdot m_p$
56	s_o+a	s_o+a-R	$\frac{a\cdot\left((s_o+a)^2+(s_o+a-R)^2\right)\cdot\delta}{((s_o+a)\cdot(s_o+d-g)-R\cdot s_o)\cdot(s_o+a)}\cdot m_p$

The internal work for the bolts at positions #3 and #4 are tabulated in Table A.4c, and are determined by finding the product of the imposed virtual displacement and the yield load of the bolt.

Summing the internal work from Tables A.4b and A.4c furnishes the total internal work. This is then equated to the external work, yielding the following expression for the moment that causes plastic collapse according to Mechanism 4:

$$M_{yl}=2\cdot\left(U_{p12}+U_{p14}+U_{p15}+U_{p23}+U_{p34}+U_{p45}+U_{p56}+U_{b3}+U_{b4}\right)\cdot\frac{d}{\delta} \qquad \text{(A.12)}$$

The expression must be minimised with respect to R to obtain the correct moment and collapse mechanism. Physical considerations dictate that the value

of R must be greater than zero and less than $(s_o + a)(s_o + g)/s_o$ to prevent yield line *56* passing above bolt hole #3.

A.6 Mechanism 5

Mechanism 5, shown in Figure A.5, consists of six yield lines coupled with yielding of the bolts at positions #3 and #4. Yield line *45* forms between the tensile corner of the section and intersects the edge of the end plate a distance of *R* from the bottom of the end plate as shown. Yield line *14* forms from the top corner of the section and intersects yield line *45* at the edge of the plate.

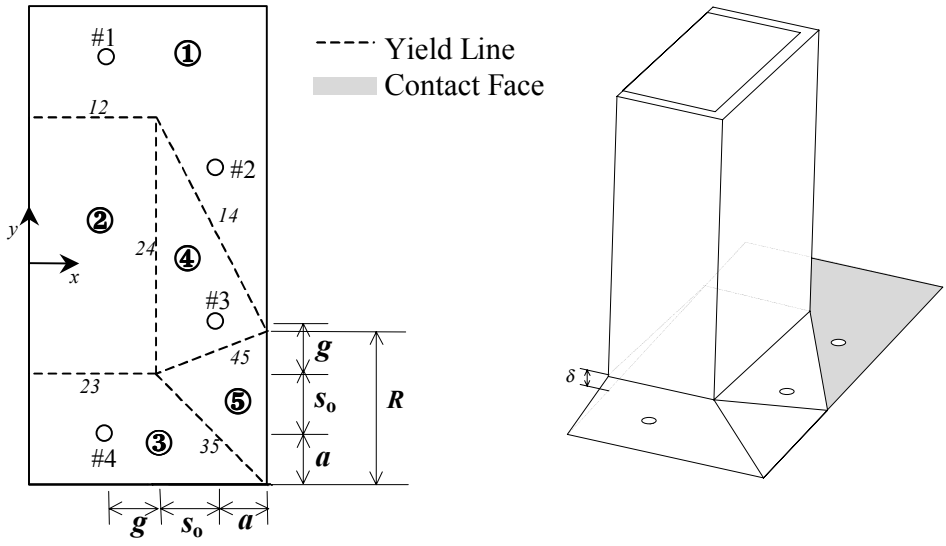

Figure A.5. Mechanism 5

Applying the virtual displacement (δ) to the tensile flange of the section enables the normal vectors of Planes 1 to 6 to be expressed as

$$\boldsymbol{n}_1 = 0\,\mathbf{i} + 0\,\mathbf{j} + \mathbf{k}$$
$$\boldsymbol{n}_2 = 0\,\mathbf{i} + \delta\,\mathbf{j} + d\,\mathbf{k}$$
$$\boldsymbol{n}_3 = 0\,\mathbf{i} - \delta\,\mathbf{j} + (s_o + a)\,\mathbf{k}$$
$$\boldsymbol{n}_4 = (s_o + a + d - R)\cdot\delta\,\mathbf{i} + (s_o + a)\cdot\delta\,\mathbf{j} + (s_o + a)\,\mathbf{k}$$
$$\boldsymbol{n}_5 = R\cdot\delta\,\mathbf{i} + 0\,\mathbf{j} + R\cdot(s_o + a)\,\mathbf{k}$$

Using Equation A.3, the virtual rotations of the yield lines are determined and presented in Table A.5a. The corresponding yield line lengths and internal work are given in Table A.5c.

Table A.5a. Virtual Rotations of Yield Lines for Mechanism 5

uvi	θ_{xuv}	θ_{yuv}
12	$\frac{\delta}{d}$	0
14	$\frac{\delta}{d}$	$\frac{(s_o + a + d - R)\cdot\delta}{d\cdot(s_o + a)}$
23	$\frac{\delta\cdot(d + s_o + a)}{d\cdot(s_o + a)}$	0
24	0	$\frac{\delta\cdot(s_o + a + d - R)}{d\cdot(s_o + a)}$
35	$\frac{\delta}{(s_o + a)}$	$\frac{\delta}{(s_o + a)}$
45	$\frac{\delta}{d}$	$\frac{(s_o + a - R)\cdot\delta}{d\cdot(s_o + a)}$

Table A.5b. Virtual Internal Work due to Bolts for Mechanism 5

Bolt #	U_{bi}
3*	$\frac{B_{y1}\cdot((s_o + a)(s_o + g) - d\cdot a - R\cdot s_o)\cdot\delta}{(s_o + a)\cdot d}$
3a*	$\frac{B_{y1}\cdot a\cdot\delta}{s_o + a}$
4	$\frac{B_{y1}\cdot a\cdot\delta}{s_o + a}$

* while $R < \left(\frac{(s_o + g)\cdot(s_o + a)}{s_o}\right)$ holds use 3, otherwise use 3a to determine the work done by Bolt 3

Table A.5c. Yield Line Lengths and Virtual Internal Work for Mechanism 5

uvi	ℓ_{xuv}	ℓ_{yuv}	U_{puv}
12	$\frac{b}{2}$	0	$\frac{b\cdot\delta}{2\cdot d}\cdot m_p$
14	$s_o + a$	$s_o + a + d - R$	$\frac{\left((s_o+a)^2+(s_o+a+d-R)^2\right)\cdot\delta}{d\cdot(s_o+a)}\cdot m_p$
23	$\frac{b}{2}$	0	$\frac{(a+s_o+d)\cdot b\cdot\delta}{2\cdot d\cdot(s_o+a)}\cdot m_p$
24	0	d	$\frac{\delta\cdot(s_o+a+d-R)}{(s_o+a)}\cdot m_p$
35	$s_o + a$	$s_o + a$	$2\cdot\delta\cdot m_p$
45	$s_o + a$	$s_o + a - R$	$\frac{\left((s_o+a)^2+(s_o+a-R)^2\right)\cdot\delta}{d\cdot(s_o+a)}\cdot m_p$

The value of R is determined by minimising the collapse moment with respect to R. The maximum value of R is defined by the point at which yield line *45* passes through the bolt hole #2 and is defined as

$$R_{max} = \frac{(d + s_o + a)\cdot s_o - (s_o + a)\cdot g}{s_o} \tag{A.13}$$

The corresponding work generated by the bolts is given in Table A.5b, where it can be noted that the work done by bolt #3 (U_{b3}) depends on the value of R.

Summing the internal work due to the plates (Table A.5c) and the bolts (Table A.5b), and equating to the external work enables the expression for the moment to cause plastic collapse of the connection to be expressed as

$$M_{yl} = 2\cdot\left(U_{p12} + U_{p14} + U_{p23} + U_{p24} + U_{p35} + U_{p45} + U_{b3} + U_{b4}\right)\cdot\frac{d}{\delta} \tag{A.14}$$

The governing moment is found by minimising the expression with respect to R. In practice this minimisation process is performed numerically.

A.7 Mechanism 6

Mechanism 6 is shown in Figure A.6. Failure occurs with a single yield line forming at the intersection of Planes 1 and 2, and all the bolts below the compressive flange of the beam section yielding.

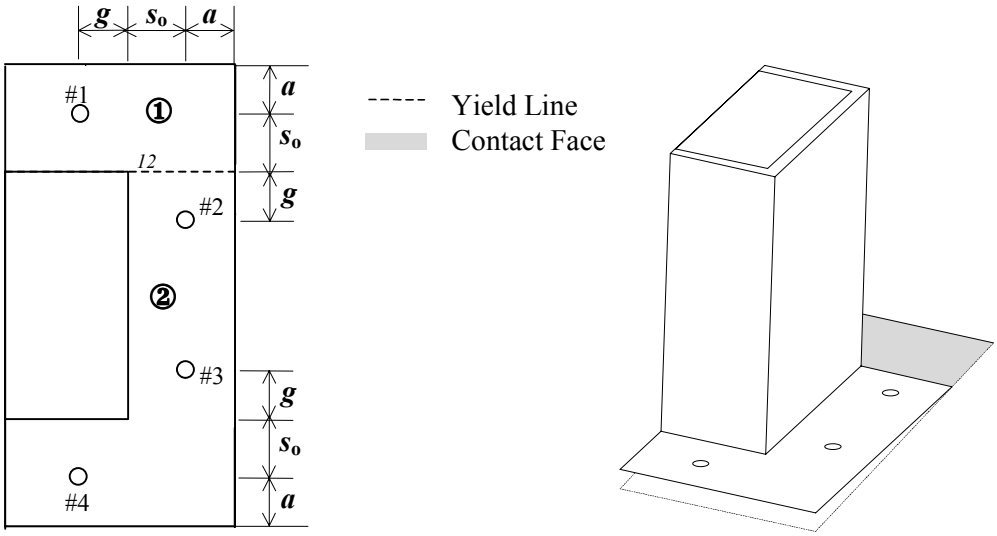

Figure A.6. Mechanism 6

The moment to cause plastic collapse of the connection is found using virtual work principles. The virtual displacement (δ) is placed along the bottom of the section, this defining the magnitude of the displacement at each bolt. The planes are expressed in terms of their normal vectors as

$$\boldsymbol{n}_1 = 0\,\mathbf{i} + 0\,\mathbf{j} + \mathbf{k}$$
$$\boldsymbol{n}_2 = 0\,\mathbf{i} + \delta\,\mathbf{j} + d\,\mathbf{k}$$

The imposed virtual displacements of the bolts are expressed as

$$\delta_2 = \frac{g \cdot \delta}{d}$$
$$\delta_3 = \frac{(d-g) \cdot \delta}{d}$$
$$\delta_4 = \frac{(d+s_o) \cdot \delta}{d}$$

The internal work generated in the end plate U_p is defined using Equations A.3 and A.5 and is expressed as

$$U_{\mathrm{p}} = \frac{(2 \cdot s_{\mathrm{o}} + 2 \cdot a + b) \cdot m_{\mathrm{p}} \cdot \delta}{2 \cdot d} \tag{A.15}$$

The corresponding work generated by the bolts U_{b} is defined by Equation A.4 and is expressed as

$$U_{\mathrm{b}} = \frac{B_{\mathrm{y1}} \cdot ((d + s_{\mathrm{o}}) + (d - g) + g) \cdot \delta}{d} = \frac{B_{\mathrm{y1}} \cdot (2 \cdot d + s_{\mathrm{o}}) \cdot \delta}{d} \tag{A.16}$$

Equating the sum of the internal work ($U_{\mathrm{p}} + U_{\mathrm{b}}$) to the external work (Equation A.6) the expression defining the moment to cause plastic collapse through Mechanism 6 can be expressed as

$$M_{\mathrm{yl}} = \left(\frac{2 \cdot s_{\mathrm{o}} + 2 \cdot a + b}{2} \right) \cdot m_{\mathrm{p}} + (2 \cdot d + s_{\mathrm{o}}) \cdot B_{\mathrm{y1}} \tag{A.17}$$

A.8 Mechanism 7

Mechanism 7, shown in Figure A.7, occurs with no yield lines forming in the end plate. The mechanism is a result of all the bolts in the connection yielding.

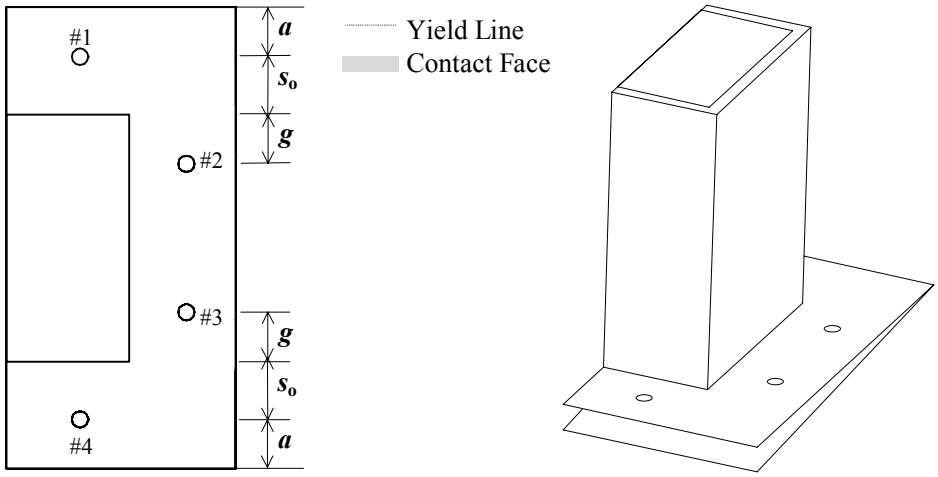

Figure A.7. Mechanism 7

Using virtual work principles and prescribing a virtual displacement (δ) on the tensile flange of the section enables the imposed virtual displacements at each bolt position to be determined as

$$\delta_1 = \frac{a \cdot \delta}{d + s_o + a}$$

$$\delta_2 = \frac{(a + s_o + g) \cdot \delta}{d + s_o + a}$$

$$\delta_3 = \frac{(a + s_o + d - g) \cdot \delta}{d + s_o + a}$$

$$\delta_4 = \frac{(a + 2 \cdot s_o + d) \cdot \delta}{d + s_o + a}$$

The internal work generated by the bolts is therefore

$$U_b = \frac{B_{y1} \cdot (2 \cdot d + 4 \cdot (s_o + a)) \cdot \delta}{d + s_o + a} \tag{A.18}$$

By equating the internal (Equation A.18) and external (Equation A.6) work, the moment to cause Mechanism 7 is expressed as

$$M_{yl} = \frac{B_{y1} \cdot (2 \cdot d + 4 \cdot (s_o + a))}{d + s_o + a} \cdot d \tag{A.19}$$